Temporal Evolution of Color Representations Measured with Magnetoencephalography Reveals a "Coarse to Fine" Dynamic

Erin Goddard[1,2] and Kathy T. Mullen[1]

Abstract

■ Color perception is based on the differential spectral responses of the L-, M-, and S-cones and subsequent subcortical and cortical computations and may include the influence of higher-order factors such as language. Although the early subcortical stages of color vision are well characterized, the organization of cortical representations of color remain elusive, despite numerous models based on discrimination thresholds, appearance, and categorization. An underexplored aspect of cortical color representations is how they unfold over time. Here, we compare the dynamic reorganization of three different color representations over time using magnetoencephalography. We measured neural responses to 14 hues at each of three achromatic luminances (increment, isoluminant, and decrement) while participants attended either to the exact color of the stimulus or its color category. We used a series of classification analyses, combined with multidimensional scaling and representational similarity analysis, to ask how cortical representations of color unfold over time from stimulus onset. We compared the performance of "higher order" models based on hue and color category with a model based simply on stimulus cone contrast and found that all models had significant correlations with the data. However, the unique variance accounted for by each model revealed a dynamic change in hue responses over time, which was consistent with a "coarse to fine" transition from a broad clustering into categorical groups to a finer within-category representation. Notably, these dynamics were replicated across data sets from both tasks, suggesting they reflect a robust reorganization of cortical hue responses over time. ■

INTRODUCTION

The first stage of human color vision is based on the combination of the differential responses of the L-, M-, and S-cones to the visual stimulus. In this first postreceptoral stage, comparisons of the cone responses are initially made within two distinct cone opponent streams, an L-/M-cone opponent response (loosely called "red-green") and one based on the opponent combination of S-cones with the other two (loosely called "blue-yellow"). On the basis of physiological and behavioral data, these two pathways are thought to remain segregated within the subcortical processing stages, using different anatomical cell types and pathways in the retina, LGN, and with distinct V1 cortical inputs (Lennie & Movshon, 2005; Derrington, Krauskopf, & Lennie, 1984). There is also evidence for a behavioral separation at detection threshold (Eskew, 2009; Mullen & Sankeralli, 1999). These two low-level pathways, however, do not provide adequate accounts of color appearance or the perceptual organization of the different colors. For example, colors that are equally spaced in a representation based on perceptual differences/similarity (e.g., using an International Commission on Illumination (CIE) L*a*b* space) vary in a nonuniform way in a space based on the relative cone responses (e.g., a cone contrast space). Furthermore, it has been widely observed that stimulating the cardinal directions of a cone contrast space, which uniquely activate one type of cone opponent process at a time, do not generate the color appearance of a unique hue. Hence, the unique hues are not aligned with the cone opponent axes and further computations are required for cone opponency to generate the full range of color appearances (Conway, Malik-Moraleda, & Gibson, 2023; Li, Garg, Zhang, Rashid, & Callaway, 2022; Stockman & Brainard, 2010; de Valois & de Valois, 1993). Embedded within this perceptual color space is a categorical organization, in which colors can be placed into groups according to their color appearance, such as the 11 basic color names of Berlin and Kay (1969). Whether there are any categorical effects in color perception, including potential interaction with language, remains controversial, but evidence is clearer for "categorical facilitation" effects, likely mediated by a shift of attention to the linguistic distinction between color categories (for a review, see Witzel, 2019). So far, the computational nature of the processes underlying categorical color grouping and subsequent color naming also remains unknown (Siuda-Krzywicka, Boros, Bartolomeo, & Witzel, 2019).

Imaging approaches provide an important route into the understanding of how colors are represented in cortex. fMRI can be used to decode stimulus color using a

[1]McGill Vision Research, Department of Ophthalmology & Visual Sciences, McGill University, Montreal, Canada, [2]School of Psychology, UNSW, Sydney, Australia

Journal of Cognitive Neuroscience 37:11, pp. 2326–2350
https://doi.org/10.1162/jocn.a.56

multivariate approach to analyze spatially distributed patterns of voxel activity in cortex (Goddard & Mullen, 2020; Brouwer & Heeger, 2009, 2013; Goddard, Mannion, McDonald, Solomon, & Clifford, 2010; Parkes, Marsman, Oxley, Goulermas, & Wuerger, 2009). Although colors can be decoded in early visual cortical areas (V1, V2, V3, hV4, and ventral occipital area [VO]), the ventral areas hV4 and VO showed a stronger perceptual relationship than earlier areas such as V1 and V2, with perceptually similar colors evoking the most similar responses (Brouwer & Heeger, 2009). Brouwer and Heeger (2013) also found that areas hV4 and VO1 showed evidence of categorical clustering, especially when participants were engaged in a color categorization task, compared with a diverted attention condition. There is also evidence of further areas of high color responsiveness more anterior in ventral visual cortex (VVC; Stoughton & Conway, 2008; Zeki & Bartels, 1999; Komatsu, Ideura, Kaji, & Yamane, 1992), including adjacent to areas associated with higher-order responses such as to objects, faces, and places (Lafer-Sousa, Conway, & Kanwisher, 2016; Lafer-Sousa & Conway, 2013).

Magnetoencephalography (MEG) signals can be used to decode stimulus color with the advantage of allowing the precise timing of the stimulus response to be determined (Hermann, Singh, Rosenthal, Pantazis, & Conway, 2022; Rosenthal, Singh, Hermann, Pantazis, & Conway, 2021). This previous work, using four stimulus colors and two luminance levels, has shown that MEG signals can be used to decode stimulus color for over 300 msec after stimulus onset (Rosenthal et al., 2021) and provides a proof of concept that similarity relationships can be used to test the geometry of stimulus color representations. Other MEG studies have also demonstrated color decoding from MEG signals (Goddard, Carlson, & Woolgar, 2022; Goddard, Shooner, & Mullen, 2022; Teichmann et al., 2020; Sandhaeger, von Nicolai, Miller, & Siegel, 2019; Teichmann, Grootswagers, Carlson, & Rich, 2019) and task-based changes in color coding consistent with sharpening of color tuning with attention (Goddard, Carlson, et al., 2022; Bartsch et al., 2017). In addition, there are many examples of decoding stimulus color from EEG signals (Bae & Chen, 2024; Grootswagers, Robinson, Shatek, & Carlson, 2024; Rozman, Chauhan, & Martinovic, 2024; Chauhan, Jakovljev, Thompson, Wuerger, & Martinovic, 2023; Retter, Gao, Jiang, Rossion, & Webster, 2023; Wu et al., 2022; Hajonides, Nobre, van Ede, & Stokes, 2021; Sutterer, Coia, Sun, Shevell, & Awh, 2021).

Here, we recorded MEG signals while participants viewed a set of 42 stimuli that varied in hue as well as achromatic offset and compared the timing of the emergence of neural representations of chromatic and achromatic information. We included two task conditions, both involving attention to the stimulus color but only one requiring color naming (categorization), to test whether the task of color naming influences the way color is represented in cortex.

To test how neural color representations evolve over time, we first used an exploratory analysis of the MEG data (multidimensional scaling [MDS]), and second, a model-driven representational similarity analysis (RSA; Popal, Wang, & Olson, 2019; Kriegeskorte, Mur, & Bandettini, 2008; Kriegeskorte et al., 2008). In the RSA, we compared three different theoretical (model) response spaces, reflecting different factors that could be influential in the neural representation of color: the cone contrast differences between the stimuli; the perceptual differences between stimuli based on color discriminability; and color category, in which within-category pairs of stimuli are predicted to produce more similar responses than cross-category ones. Our results show an orderly representation of hue across the stimulus-induced response that is broadly consistent with each of the three a priori models above. Interestingly, we find a nonlinear warping of the representational space that is dynamic, changing over time from the stimulus onset. These nonlinearities suggest a "coarse to fine" dynamic, in which the cortical hue representation includes an initial clustering of similar hues before a later separation of these clusters to represent the finer differences between stimuli. We replicated the dynamics of these hue representations across the data from the two different tasks and finding only a subtle indication of possible task-mediated differences in the later part of the response.

METHODS

Participants

We collected MEG data on eight participants (five female, three male, aged 21–34 years, mean = 26.4 years). Each participant had no history of neurological and/or psychiatric disorders, normal or corrected-to-normal visual acuity, and normal color vision as assessed with Ishihara plates (Ishihara, 1990) and the Farnsworth-Munsell 100-hue test (Farnsworth, 1957). All participants provided informed consent before taking part, and all experimental procedures were approved by the ethics review board of the McGill University Health Centre and were conducted in accordance with the Declaration of Helsinki. We collected MEG data for each participant during a single session, of approximately 2 hr. Each participant was familiarized with all tasks before the day of the MEG data collection, but all behavioral data reported here are from the MEG session.

Our sample size (n = 8) is smaller than previous work testing for color representations with MEG (n = 18; Hermann et al., 2022; Rosenthal et al., 2021), but larger than earlier work using fMRI (n = 5, Brouwer & Heeger, 2009, 2013), and larger than our recent MEG work, which included similar analysis approaches (n = 6; Goddard, Shooner, et al., 2022). Teichmann, Moerel, Baker, and Grootswagers (2022) used real and simulated data to test the effect of participant and trial numbers on statistical

power for classification analyses of MEG responses to visual stimuli. They report that sufficient data at a subject level (i.e., enough trials) is likely more important for statistical power than sample size, giving the empirical example of a data set with nine participants completing 1600 trials having equivalent power to data from 18 participants who completed 400 trials. In this study, we prioritized many trials (>3,800 trials per participant) to increase this subject-level power.

Visual Stimuli

All visual stimuli were large circular patches of uniform color, serially presented. Each circular stimulus was 40° in diameter, presented in a raised-cosine envelope, and outside the stimulus area, the screen was set to a gray of mean luminance, as illustrated in Figure 1. We used 14 hues, chosen to be equally spaced around a circle of diameter 40 in the isoluminant plane of CIE Lab space. The saturation of the stimuli was chosen to be close to the maximum achievable within the gamut of the display.

We determined the isoluminant plane of CIE Lab space for each participant individually using heterochromatic flicker photometry (He, Taveras Cruz, & Eskew, 2020; Smith & Pokorny, 1975). At the start of the experimental session, participants viewed a sinusoidally flickering stimulus, alternating between a frame of a colored stimulus (as in Figure 1B) and an achromatic stimulus of the same spatial properties. Participants used a mouse to adjust the luminance of the achromatic stimulus until their impression of flicker was minimized, indicating their selection with a mouse click. After performing at three settings for each of the 14 hues, we averaged the selected luminances for each hue. We fit a sinusoid to these average offsets across hue direction, with amplitude and phase as fitted parameters and used the fitted values to adjust the experimental stimuli for perceptual isoluminance. Across participants, the phase of the fitted sinusoid aligned with stimulus hue such that the maximum correction was applied to the stimuli closest to the L-M isolating axis, as expected for a correction to adjust for individual variability in the luminance mechanism. The maximum amplitude of this achromatic correction (L = M = S) varied across individuals (range: 0.8–4.9%, mean: 2.9% cone contrast). In addition to the 14 hues that were isoluminant with the background, we used another 28 hues that were of the same hue direction but with a 12.5% luminance increment or decrement, giving 42 unique stimuli.

After the stimuli were calibrated for their individual perceptual isoluminance, participants viewed all stimuli sequentially and verbally reported the color category of each stimulus, which were recorded by the experimenter. Participants were restricted to using the labels "red/pink," "orange," "yellow," "green," "blue," and "purple." Each stimulus was presented 3 times, totaling 126 trials. The modal color labels for each unique stimulus were used to define each participant's color categories, used in the category task (described under "participant task" below) and the category model (used in the RSA, described below).

No MEG data were collected during these preliminary tasks.

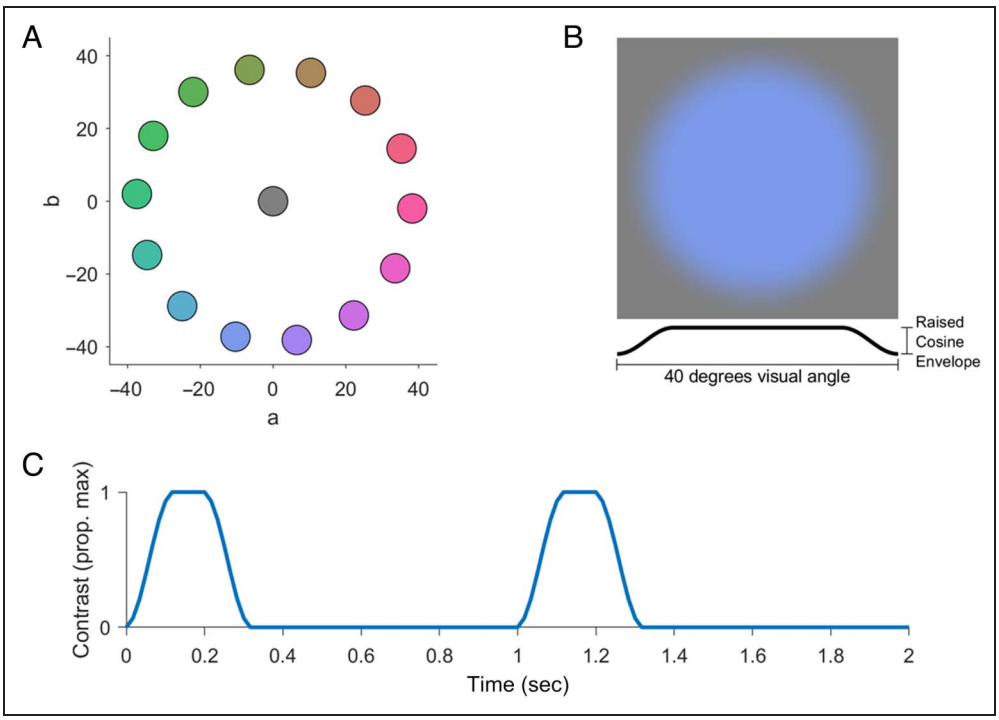

Figure 1. Spatial and temporal stimulus properties. (A) Stimuli were 14 hues, equally spaced around a circle in the isoluminant plane of Lab space, presented at three luminance levels (not shown here). The background was held at mean gray (a = b = 0). (B) Each stimulus was a color presented in a circular raised-cosine spatial envelope. (C) Example timecourse of two trials: Each stimulus was presented in a temporal raised-cosine envelope.

MEG Methods: Acquisition Protocols

MEG data were collected with a whole-head MEG system (CTF OMEGA System) consisting of 275 axial gradiometers. For each MEG session, we first collected 5 min of empty room recordings, which we used to estimate noise covariance of the sensors (see below). Before the participant entering the magnetically shielded room, three marker coils were placed on the participant's head. Marker positions, nasion, left and right pre-auricular points, and the participant's head shape were recorded with a pen digitizer (Polhemus Isotrak), using a minimum of 500 points. Two EOG electrodes were places above and below the left eye, to record eye blinks and eye movements during the MEG session. Two electrodes were placed across the plane of the chest to collect electrocardiographic signals, and a reference electrode was placed below the participant's collarbone. Each participant's MEG data and simultaneous EOG and electrocardiographic signals were collected at a sampling frequency of 2400 Hz. In conjunction with these data, we collected participants' button responses using a VPixx ResponsePixx button box system (VPixx Technologies).

MEG Methods: Display Apparatus and Calibrations

We displayed stimuli using a PROPixx DLP LED projector (VPixx Technologies, resolution 1920 × 1080), located outside the magnetically shielded room, to back-project images onto a custom screen via two mirrors. Participants, lying supine in the MEG system, viewed the custom screen, located above them, from a distance of 45 cm. We used a Windows PC (Windows 7) running MATLAB (R2017a) in conjunction with routines from Psychtoolbox 3.0 (Kleiner, Brainard, & Pelli, 2007; Brainard, 1997; Pelli, 1997) to generate and project the stimuli (refresh rate 60 Hz, mean luminance 106 cd/m^2). The PROPixx DLP LED projector has a linear gamma and was color calibrated as described previously (Mullen, Dumoulin, & Hess, 2008; Mullen, Dumoulin, McMahon, de Zubicaray, & Hess, 2007; Michna, Yoshizawa, & Mullen, 2007). We precisely aligned stimulus presentation times with the recorded MEG data using the VPixx "Pixel Mode" to record the output of a single pixel along with the MEG data.

MEG Methods: Experimental Design and Participant's Task

Each participant completed the MEG data collection in a single session, which was divided into 10 blocks of 5–7 min each, with breaks between blocks. On each block of trials, participants saw the same stimulus set (summarized in Figure 1) and performed a 1-back task requiring color categorization or discrimination. In both tasks, the spatial and temporal properties of the stimuli were identical, with each trial comprising a single color presented in a temporally raised-cosine envelope (300 msec in total, with 100 msec onset, 100-msec sustained presentation, and 100 msec offset). Across both tasks, the trials were presented in a continuous stream, and participants responded with a keypress whenever two consecutive stimuli were an exact match (discrimination task) or a color category match (category task, where same category was defined as stimuli that were given the same label in the color naming task).

For both tasks, we used at least 42 trials of each of the 42 unique stimuli (1764 trials). These were presented in a counterbalanced order where each stimulus was preceded by each of 42 stimuli at least once. Because category matches were more common than exact stimulus matches, we added extra exact match trials to the discrimination task blocks so that the average rate of match trials was the same across the two tasks. The total number of trials in the discrimination task ranged from 2066 to 2130 across participants, because the match rate in the category task varied with their individual color labels.

In pilot testing, participants were faster and more accurate for the discrimination task than for the category task: To approximately equate the tasks for difficulty in the experiment, we used a longer ISI in the category task (700 msec) than in the discrimination task (450 msec), giving stimulus onsets that were separated by 1000 msec and 750 msec, respectively.

For both the category and the discrimination tasks, we evaluated participants' performance using their hit rate (proportion of match trials with a button press) and false alarm rate (proportion of nonmatch trials with a button press) to calculate sensitivity (d') using the MATLAB function *norminv* (inverse of the cumulative normal distribution):

$$d' = norminv(\mathrm{HR}) - norminv(\mathrm{FA})$$

All participants performed these tasks well above the chance rate of $d' = 0$. Across participants, the average $d' = 2.7$ (range $d' = 1.8$–4.1) on the category task, and $d' = 3.3$ (range $d' = 2.4$–4.2) on the discrimination task.

MRI Methods: Retinotopic and Functional Localizers

Each participant completed an MRI session in which we acquired high-resolution anatomical images of their brains and functional data used to define ROIs. All magnetic resonance imaging took place at the McConnell Brain Imaging Centre, McGill University, Montreal, Canada. For each participant, we acquired two high-resolution three-dimensional whole head T1 images using an magnetization prepared rapid gradient echo sequence (inversion time = 900 msec, repetition time = 2300 msec, echo time = 3.41 msec, 1.0-mm^3 resolution) and averaged these two images to generate the participant's anatomical template. Functional T2* MR images were acquired on a 3 T Siemens MAGNETOM Prisma system with a 32-channel head coil. Gradient-echo pulse sequences were used to

measure BOLD signal as a function of time. We identified the visual cortical regions V1, V2, V3, V3A/B, LO1/LO2, and hV4 for each participant using rotating wedge stimuli and expanding and contracting concentric rings (Sereno et al., 1995; Engel et al., 1994), standard definitions of these areas (Goddard, Mannion, McDonald, Solomon, & Clifford, 2011; Larsson & Heeger, 2006; Brewer, Liu, Wade, & Wandell, 2005), and the foveal confluence (Schira, Tyler, Breakspear, & Spehar, 2009). To localize areas VO1, VO2, and human middle temporal area (hMT+), we used data from the retinotopic mapping scans in conjunction with functional localizers for VO (Mullen et al., 2007) and hMT+ (Huk, Dougherty, & Heeger, 2002). Full details of our retinotopic mapping procedures, including scanning protocols, data preprocessing, and area definition have been described previously (Goddard, Chang, Hess, & Mullen, 2019).

MEG Data Analysis: Preprocessing and Source Reconstruction

Preprocessing, forward modeling, and source reconstruction of MEG data were performed using Brainstorm (Tadel, Baillet, Mosher, Pantazis, & Leahy, 2011, https://neuroimage.usc.edu/brainstorm). For each participant's template anatomical (a high-resolution MRI image), we used the automatic segmentation processes from Freesurfer 6.0 (Dale, Fischl, & Sereno, 1999; Fischl, Sereno, & Dale, 1999) to define the gray/white matter and pial/gray matter boundaries. Using Brainstorm, we imported the output of Freesurfer and created a 15,000-vertex model of each participant's cortical surface. For each block of trials in the MEG data, we aligned the participant's cortical surface model to the median measured marker coil locations for that block by aligning the head shape data from the MRI with the head shape relative to the marker coils, as recorded with the pen digitizer. For each functional run, we generated a forward model for each model by applying a multiple spheres model (Huang, Mosher, & Leahy, 1999) to the participant's cortical surface model at this measured head location.

Functional data were preprocessed in Brainstorm with notch filtering (60, 120, and 180 Hz), followed by bandpass filtering (0.2–200 Hz, using the Brainstorm default of an even-order linear phase finite impulse response filter). We preprocessed data from the empty room recording using identical protocols and then used the output to estimate the noise covariance for the session. Cardiac and eye blink artifacts were removed from functional data using signal space projection. Cardiac and eye blinks events were identified using default filters in Brainstorm, manually verified, and then used to estimate a small number of basis functions corresponding to these noise components, which were removed from the recordings (Uusitalo & Ilmoniemi, 1997). From these functional data, we extracted an epoch of data for each trial: from −100 to 1000 msec relative to stimulus onset and downsampled to 200 Hz. Using the noise covariance estimate, regularized using the median eigenvalue, we applied a minimum norm source reconstruction to this trial data.

For classification analyses, we generated three data sets using each participant's functionally defined cortical areas, as in previous work (Goddard, Shooner, et al., 2022). In "early visual cortex" (EVC) ROI, we included data from all vertices located within areas V1, V2, and V3, whereas the VVC ROI included areas hV4, VO1, and VO2, and "dorsolateral visual cortex" (DVC) included areas V3A/B, LO1, LO2, and hMT+. We found very similar effects across these ROIs, which we believe most likely reflects the failure of the source reconstruction to completely isolate responses from these adjoining cortical regions. Because there is little difference across ROIs, below, we show data from EVC only, but equivalent figures for VVC and DVC are included in the Appendix.

MEG Data Analysis: Classification-based Analyses

We used a series of classification analyses to measure the amount of information about stimulus color and luminance that was available in the neural responses, as measured with MEG. We repeated these analyses for each 5-msec bin to capture how this information changed over time. Out of the total 15,000 sources in each participant's head model, the EVC ROI included an average of 731 sources (SD = 165), the VVC ROI included an average of 396 sources (SD = 67), and the DVC ROI included an average of 434 sources (SD = 106). We reduced these with PCA and retained data from the first n components, which accounted for 99.9% of the variance, for the classification analysis (mean = 285.9, SD = 13.7 for EVC; mean = 283.6, SD = 17.4 for VVC; mean = 283.6, SD = 20.5 for DVC).

We conducted a series of pairwise classifications based on either stimulus hue or stimulus luminance, with separate analyses for data from the category and discrimination tasks, and for each ROI. In each case, we trained classifiers to discriminate between two categories of trial (i.e., two hues or two luminance levels) and tested on held-out data. We report results obtained with a linear support vector machine classifier, using the MATLAB function *fitcsvm* with *KernelFunction* set to *linear*. For all analyses, we expressed average classifier accuracy in d' (a unit-free measure of sensitivity). Chance classification performance yields $d' = 0$.

For classification analyses, we generated "pseudo-trials" to increase signal-to-noise ratio along the dimension of interest and to reduce data variability due to stimulus dimensions orthogonal to the dimension of interest (e.g., Goddard & Mullen, 2021). When training classifiers to discriminate stimulus hue, we used pseudotrials that were each the average of 12 trials of the same hue: 4 of each luminance level. Trials were sampled without replacement to ensure that each pseudotrial was composed of independent data. For data from a single task, this yielded 11 pseudotrials for each of the 14 hues. For

each pair of hues, we used these pseudotrials in an 11-fold cross-validation, in each case training on data from 20 pseudotrials (10 from each hue) and then testing the classification rule on its classification on the held-out pair of pseudotrials. We repeated this entire process 10 times, with different partitions of the data into pseudotrials. We performed an equivalent procedure when classifying stimulus luminance: generating pseudotrials that were each the average of 14 trials of the same luminance, 1 of each stimulus hue. This yielded 42 pseudotrials for each of the 3 luminance levels, and for each pair of luminance levels, we used a 42-fold cross-validation.

For both hue and luminance, we performed these classification analyses on data from within each 5-msec time bin to see how information about these stimulus features in the neural responses unfolded over time. For decoding of stimulus hue in the EVC ROI, we additionally tested for cross-temporal generalization: training classifiers on data from one time bin and then testing this classification rule on data from each later time bin in held-out pseudotrials.

MEG Data Analysis: RSA and MDS

When decoding stimulus hue, pairwise comparisons of the 14 unique hue directions resulted in a 14 × 14 dissimilarity matrix (DSM) for each time bin where each cell of the matrix was defined by classifier accuracy. To visualize how the neural representations of color were unfolding over time, we used MDS to reduce these matrices to the best-fitting two-dimensional representation of the 14 hues. Each MDS was completed using the MATLAB function *mdscale* with *criterion* set to *metricstress* (minimizing the stress normalized with the sum of squares of the dissimilarities).

We also used RSA (Nili et al., 2014; Kriegeskorte, Mur, Ruff, et al., 2008) to compare these matrices with three a priori models, based on different representations of stimulus hue (Figure 2). Each of these models predicted that the dissimilarity of the neural responses would be proportional to the stimulus difference, but with stimulus difference quantified in three possible ways: as Euclidian distance between stimuli in cone contrast (Figure 2A), CIE L*a*b* space (Figure 2B), or in color category (Figure 2C). For each time bin, we rank-correlated each participants' observed DSM with each of these three models. We compared model performance against the benchmark of the "noise ceiling," which estimates the expected correlation of the observed data with a hypothetical (unknown) "true" model, given the noise in the data (Nili et al., 2014). The upper bound of the noise ceiling is calculated by correlating the group average DSM at each time bin with each individual's DSM, which, due to overfitting, will overestimate the true model's correlation. The lower bound of the noise ceiling is calculated by correlating each individual's data with a group average that excludes their own data, avoiding overfitting, and providing a lower bound on the expected correlation with the true model.

Because our a priori models are positively correlated with each other (see legend of Figure 2 for correlation values), they will tend to covary in their correlation with the data. To estimate the extent to which these models predicted unique variance in classifier performance, we fit a series of general linear models (GLMs). For each GLM, we used the three models as regressors, applying

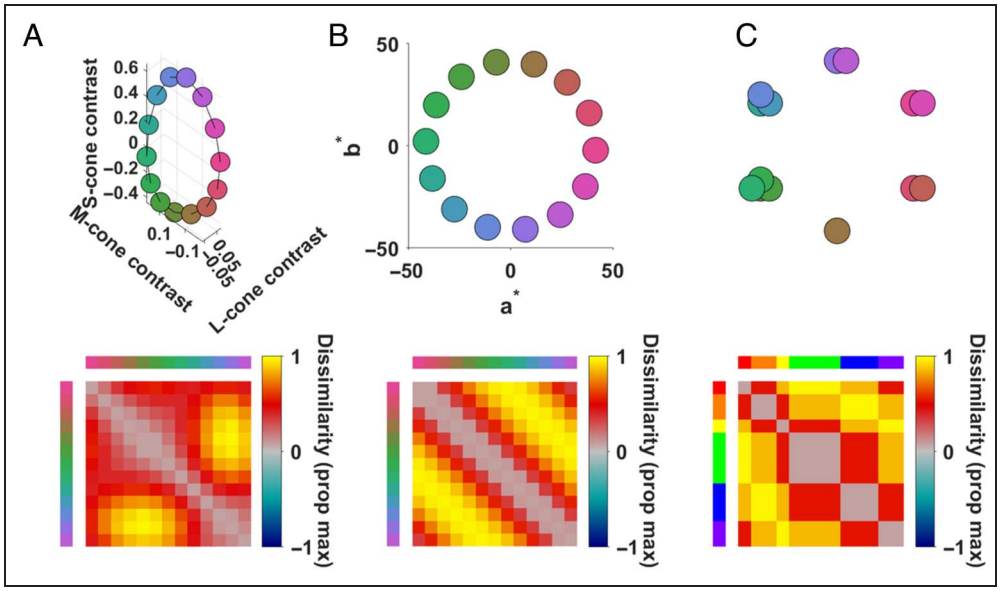

Figure 2. Model DSMs based on hue for RSA. We tested classifier data against three models of dissimilarity for the 14 stimulus hues, based on stimulus cone-contrast (A), hue direction in CIE L*a*b* space (B), or color category (C). In each case, the upper plot indicates the stimulus representation according to the relevant model, and the low plot shows the corresponding model DSM. The hues were selected to be equally spaced in CIE L*a*b* space (B); when replotted in a cone contrast space (A), the hues are not equally spaced but elongated along the S-cone contrast axis, whereas the category model (C) treats within-category hues as identical, grouped into six clusters equally spaced around a circle. The category model shown above (C) is an example model for one participant; in the analysis, each participant's color naming data were used to generate an individual category model. These three models were positively correlated with one another, Spearman's rho $r = 0.72$ (cone contrast vs. hue), $r = 0.25$–0.44 (cone-contrast vs. category), $r = 0.68$–0.73 (hue vs. category), with variation in correlation with the category model due to interparticipant variation in color naming.

spm_orth.m (from SPM12, www.fil.ion.ucl.ac.uk/spm/doc) to perform recursive Gram-Schmidt orthogonalization (Golub & Loan, 1996) of these regressors so that the final regressor would only capture variance that is predicted by the final model and orthogonal to the other two models. We then converted each data matrix to ranked classification accuracy values and fit these ranks with a GLM composed of the orthogonalized regressors, using the MATLAB function *fitglm.m*. We repeated this process three times, so that each model was the final regressor in one GLM, providing the parameter estimates (beta weights) that indicated any unique variance captured by this model.

When decoding stimulus luminance, the pairwise comparisons resulted in a 3 × 3 DSM. We conducted an RSA on these data, testing the data on two models, based either on luminance intensity or luminance contrast. Both models are shown in insets in Figure 5.

Statistical Analyses

To test whether classifier accuracy was above chance and to test whether model correlations and parameter estimates (beta weights) were above zero, we used Bayes Factor analyses, an alternative to the traditional frequentist approach (Morey & Wagenmakers, 2014; Kass & Raftery, 1995). A Bayes Factor compares evidence for competing hypotheses; here, we report where there is moderate (BF > 3) or strong (BF > 10) evidence in favor of the alternate hypothesis, or at least moderate (BF < 1/3) evidence in favor of the null hypothesis. We implemented all Bayes Factor analyses using a MATLAB package (Krekelberg, 2021).

RESULTS

We recorded MEG data while participants viewed a series of colored stimuli and performed either a categorization task or a discrimination task. During both tasks, reconstructed sources were focused in visual cortex and showed similar average event-related fields over time (Figure 3). To quantify the stimulus-related information present in the pattern of response across cortex and to explore how neural representations of stimulus hue and luminance unfolded over time, we used a series of classification analyses.

Classification of Stimulus Hue and Luminance

In Figure 4, we show the average classifier accuracy, collapsed across all pairwise comparisons, when decoding hue and luminance. Across the two tasks, we found qualitatively similar timecourses of average classifier decoding for both stimulus features, with a trend toward higher classifier accuracy in the category task.

This tendency for higher classifier accuracy in the category task may reflect the longer ISI for the category task (700 msec) compared with the discrimination task (450 msec), which we included to better match the tasks for difficulty (see the Methods section for details). The

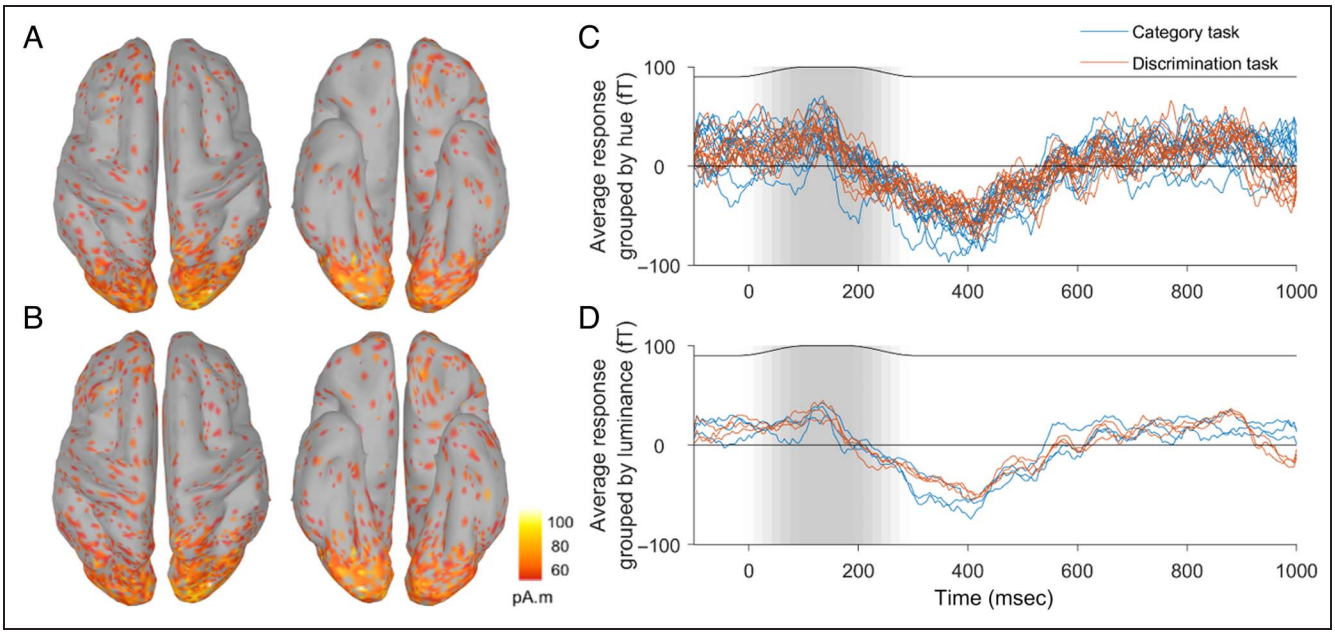

Figure 3. Estimated distributed source amplitudes (root mean square values), averaged (n = 8) for category (A) and discrimination (B) tasks, projected onto a partly inflated template cortical surface, viewed from above (left) and below (right). In C and D, the average response (event-related fields) across eight participants and all sensors is plotted, grouped by the 14 stimulus hues (C) or three luminance levels (D). Thin black lines in the upper part of each plot in C and D, along with the shaded gray background, indicate the temporal envelope of the stimulus, relative to trial onset.

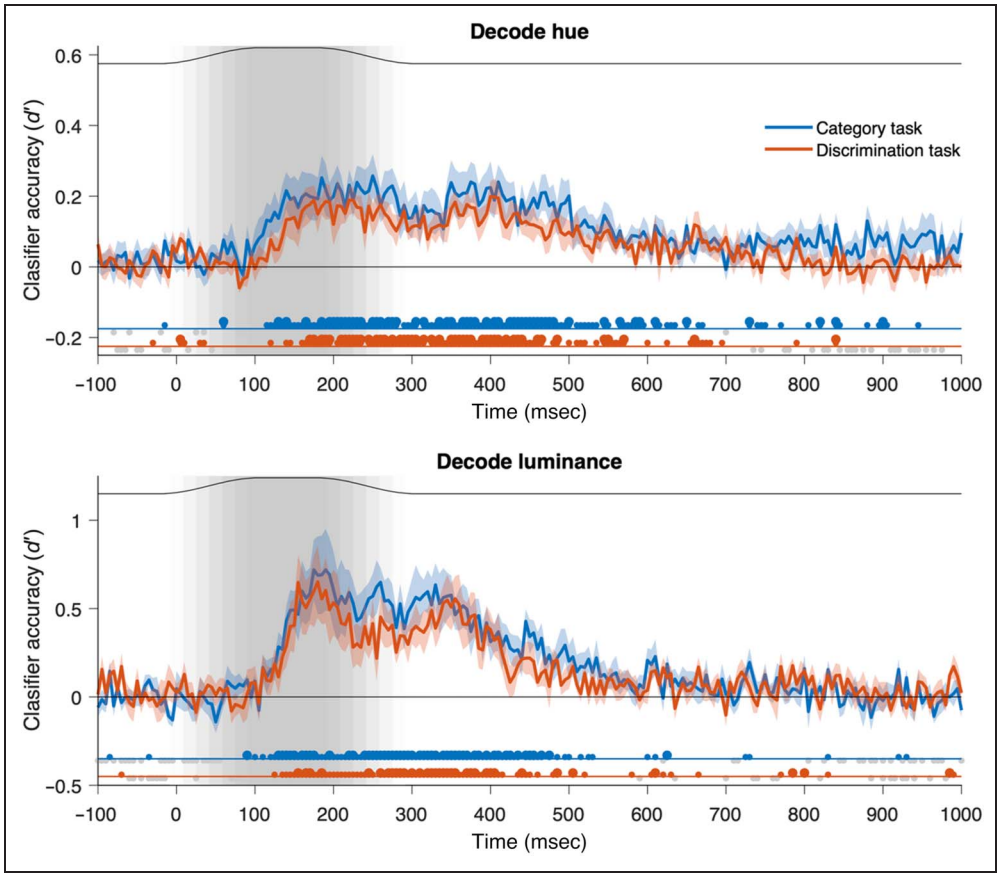

Figure 4. Decoding of stimulus hue (upper) and luminance (lower). Average classifier accuracy (n = 8) across the two tasks is shown for classification of hue and luminance. Error bars are standard errors of the between-subject means. Thin black lines in the upper part of each plot, along with the shaded gray background, indicate the temporal envelope of the stimulus, relative to trial onset. Dots below the x axis indicate the results of the Bayes Factor analyses. Colored dots show times when the classifier performance was above chance (small dots indicate moderate evidence BF > 3, large dots indicate strong evidence, BF > 10). Small gray dots indicate times where there was at least moderate evidence in favor of chance performance (BF < 0.3).

onset of above-chance decoding was approximately 100–120 msec after stimulus onset in each case, which is slightly later than reported previously (e.g., Hermann et al., 2022). This later onset is likely because our stimuli did not onset abruptly but ramped on gradually, as shown in Figure 4.

Trend toward Achromatic Contrast, Rather Than Intensity, in Luminance Decoding

Our stimuli were presented at three luminance levels: luminance decrements, stimuli isoluminant with the background, and luminance increments. If the neural responses were primarily driven by the luminance intensity differences between these, then discriminating increments versus decrements should lead to the highest classifier performance. However, if the neural responses to these stimuli were driven by luminance contrast more than intensity, then classifier performance should be highest when responses to the isoluminant stimuli are compared with either increments or decrements. These predictions are shown in the model DSMs (Figure 5, insets). Representational similarity analyses of the luminance decoding data are shown in Figure 5.

For both the category and the discrimination task, the data tended to be more consistent with the model based on achromatic contrast, rather than intensity. However, these effects were not particularly robust, as seen in the results of the Bayes Factor analysis in Figure 5. The average DSMs in Figure 5 are shown for four time windows to match those used for the hue analysis (see the next section). Across these time windows, the average DSMs are consistent with the contrast model rather the intensity model across the first three time windows shown (110–455 msec), with the lowest classifier performance for increments versus decrements in each case, but there was moderate variability across participants, which is seen in the standard error of the model correlations. The inter-participant variability is also seen in the noise ceiling, where the lower bound is not consistently above zero at time bins where there was above-chance classifier performance (as seen by comparing the dotted lines in Figure 5 with the average decoding of luminance in Figure 4). In these ways, these data are consistent with neural responses being driven by achromatic contrast, rather than intensity, but they provide only modest support for an effect in this direction.

Dynamics of Hue Representations Are Consistent across Task

Because each participant viewed stimuli of 14 different hues, the pairwise classifications of stimulus hue included 84 different comparisons. We include the average DSMs

based on hue decoding for four time windows (see Figure 6). To better visualize the stimulus representations suggested by these DSMs, we also include MDS solutions based on each of these DSMs. When the DSMs are reduced with MDS, the resultant 2-D solutions do not capture all information that may be present in the DSM. However, there is a reasonable a priori prediction that the neural representation of hue will be close to 2-D, and the 14 stimulus hues can be represented in a number of different 2-D spaces (such as the a*b* plane of L*a*b* space). In this way, the MDS solutions provide a useful insight into how the neural representations are structured if we assume that they are 2-D. To test how well each MDS solution captured the corresponding DSM, in each case, we rank-correlated (Spearman's rho) the original DSM with a distance matrix defined by the best-fitting 2-D MDS solution (Mantel test). These values were similarly high across time windows (see Figure 6).

We selected the four time windows in Figure 6 (also used in Figure 5) as equal-duration periods that together span the times with above-chance classification of stimulus hue. We chose to divide this period into four time windows to visualize the dynamics indicated by the RSA results (reported below), particularly the suggestion of a reorganization at around 300–350 msec after stimulus onset. For an alternate visualization, with shorter time windows that span the entire timecourse, we also include movies of the MDS solutions for each 50-msec time window in the Appendix.

In comparing the DSMs and MDS solutions in Figure 6 with the model predictions in Figure 2, none of the time windows in either task provide a clear match to any of the three a priori models. Nonetheless, there are several features of the data that suggest that they reflect meaningful structure and can provide insight into how the neural representation of hue unfolds over time, including features that concur with one or more of the a priori models. For instance, all three models predict that classifier performance will tend to increase as hue difference increases, and this is consistent with all observed DSMs, which have

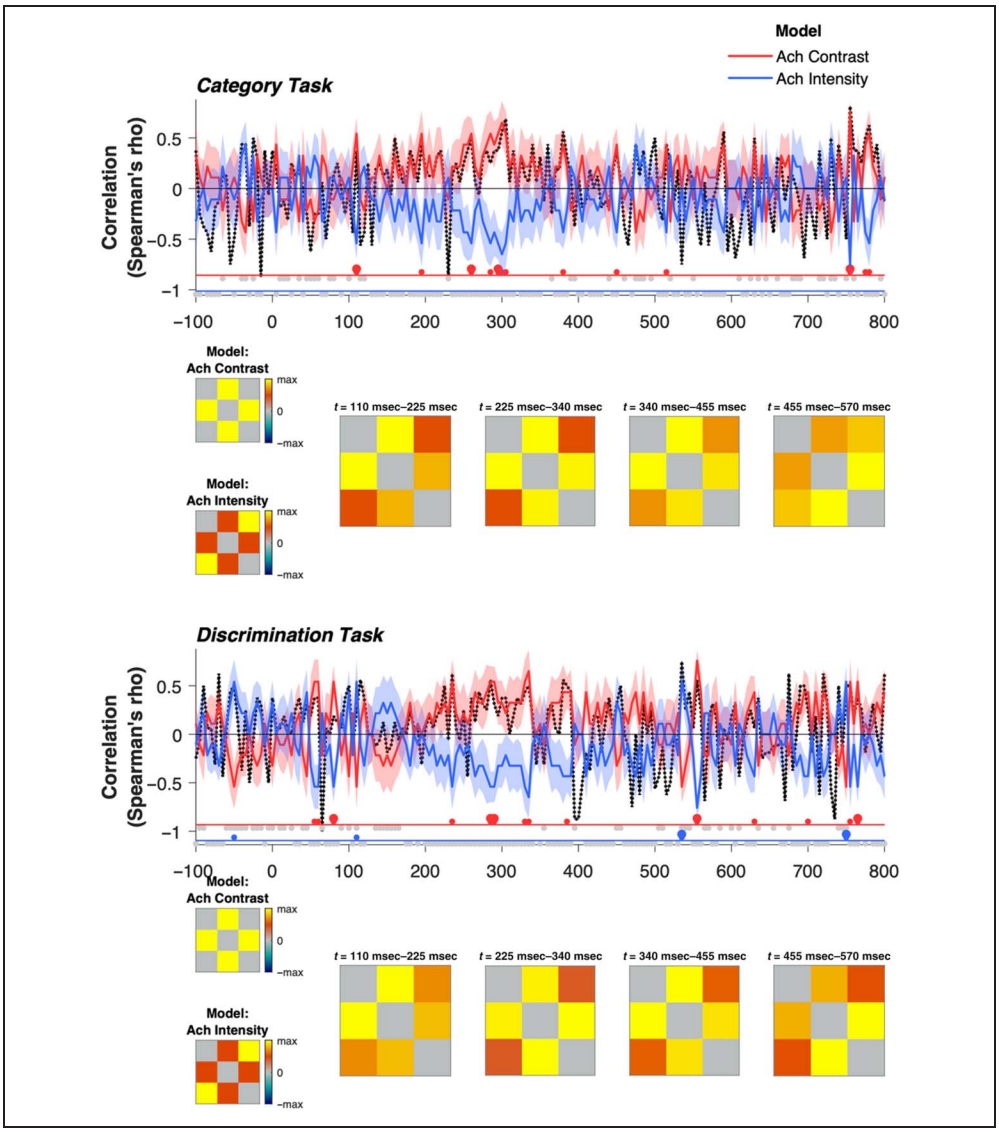

Figure 5. RSA of stimulus luminance, for the category (upper) and discrimination (lower) tasks. Average correlations (n = 8) with the achromatic contrast and intensity models, along with the average DSMs for four time windows (using the same time windows as in the reporting of hue RSA, below). Note that the achromatic contrast versus intensity models (shown in insets at the left) are perfectly negatively correlated, so the model correlations are mirror symmetrical about the x axis (time axis) and positive correlation with one model will drive negative correlation with the other. The lower bound of the noise ceiling (Nili et al., 2014; see the Methods section) is indicated by the dashed black line. Error bars are standard errors of the between-subject means, and dots below the x axis indicate the results of the Bayes factor analysis, with plotting conventions as in Figure 4.

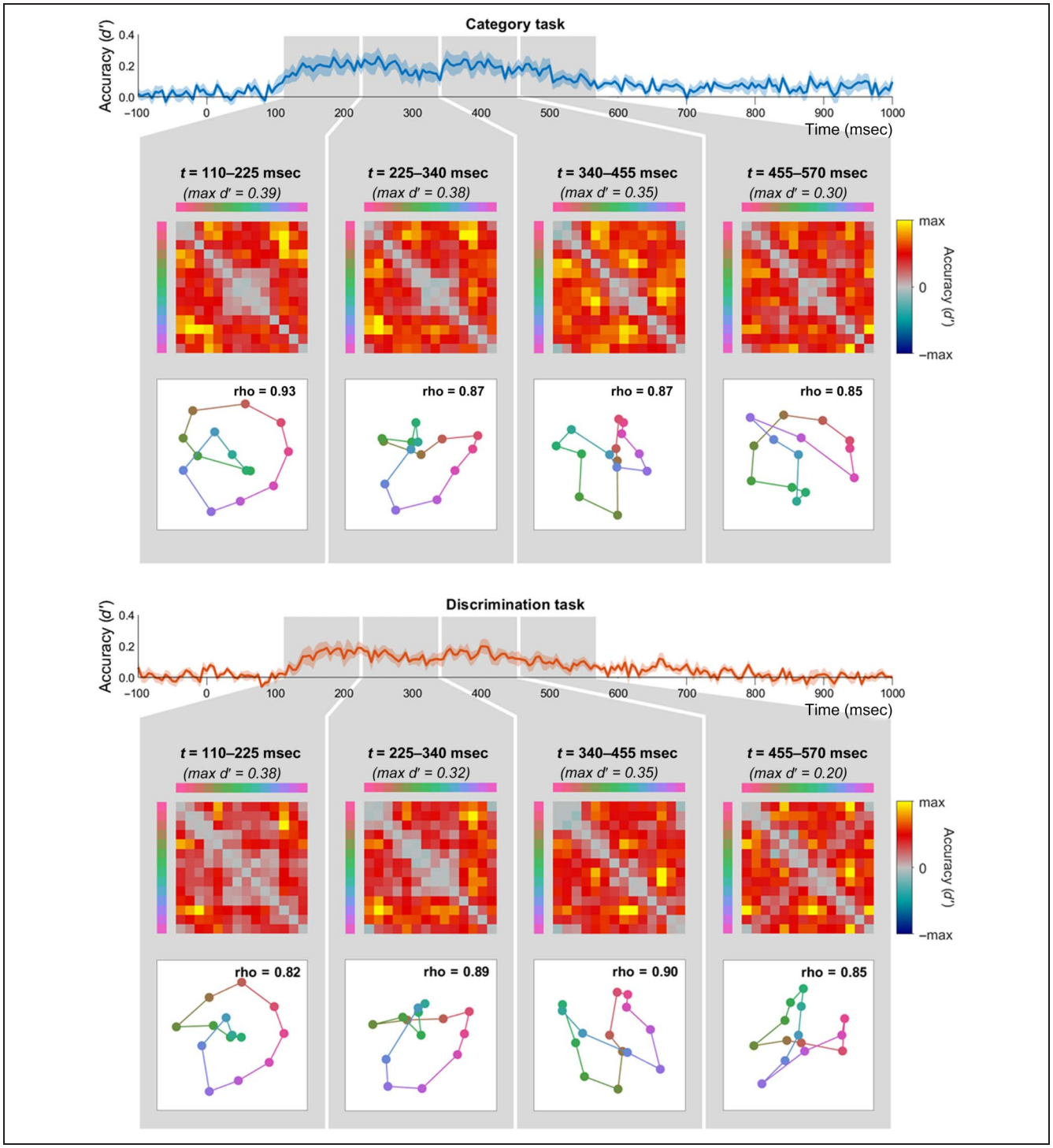

Figure 6. Average DSMs and corresponding MDS solutions for data from the category task (upper) and discrimination task (lower). In each case, we considered data from four time windows of 115 msec each, spanning the times that included above-chance classification of hue for both tasks. In both cases, the average decoding of hue (d') is replotted from Figure 4, and gray shaded regions indicate the time windows corresponding to the four DSMs. The colormap used to plot each DSM is scaled by the maximum d' of each matrix, indicated above each DSM. In the upper right of each MDS plot, rho values indicate the DSM/MDS correlation (Mantel test; see text for details).

relatively low classifier performance (close to gray) around their negative diagonals. In the MDS solutions, this is seen in tendency for hues to be arranged in order according to physical similarity (albeit with some clustering and/or folding).

For both the category task and discrimination task data, there is an evolution of the hue representation over time, as seen in the differences across the four time windows in Figure 6. The most striking feature of the data in Figure 6 is that this evolution across time windows is remarkably

consistent for data from different tasks, particularly across the first three time windows. This is notable given that data for the two tasks were collected across different MEG recordings. This replication indicates a reliable but dynamic structure in the neural representations of hue, reflecting a reorganization of hue responses over time.

In the first two time windows of Figure 6, there is relatively low classifier performance among green hues: This is seen in the squares of gray in the DSMs, and the clustering of the greens in the MDS solutions. Interestingly, the greens do not remain clustered across the entire stimulus-induced response but show greater spacing in the third time window of Figure 6. This pattern is replicated across both tasks. In the third time window, MDS solutions from both tasks include a more substantial deviation from a circular arrangement, forming a "figure of 8" with a crossing point around blue/yellow. Although the exploratory nature of these analyses precludes strong conclusions, they present interesting avenues for future work, as discussed in the general discussion below.

RSA Suggests a "Coarse to Fine" Transition in Color Representations

To better characterize how these hue representations change over the course of the stimulus-induced response, we performed an RSA, comparing the data with models based on cone contrast differences, hue difference, and color category (Figure 7) for data from both the discrimination and category tasks. All three models performed well overall (Figure 7A), with similar timing, which likely reflects the substantial overlap in their predictions based on their intermodel correlations (see Figure 2). Bayes Factors revealed moderate or strong effects across most times when classification of hue was above chance, and average model correlations that approached the lower-bound of the noise ceiling in each case. The strong performance of all three models we considered (Figure 7A) suggest a possible ceiling effect, where the shared predictions of these correlated models may account for performance approaching the lower bound of the noise ceiling across

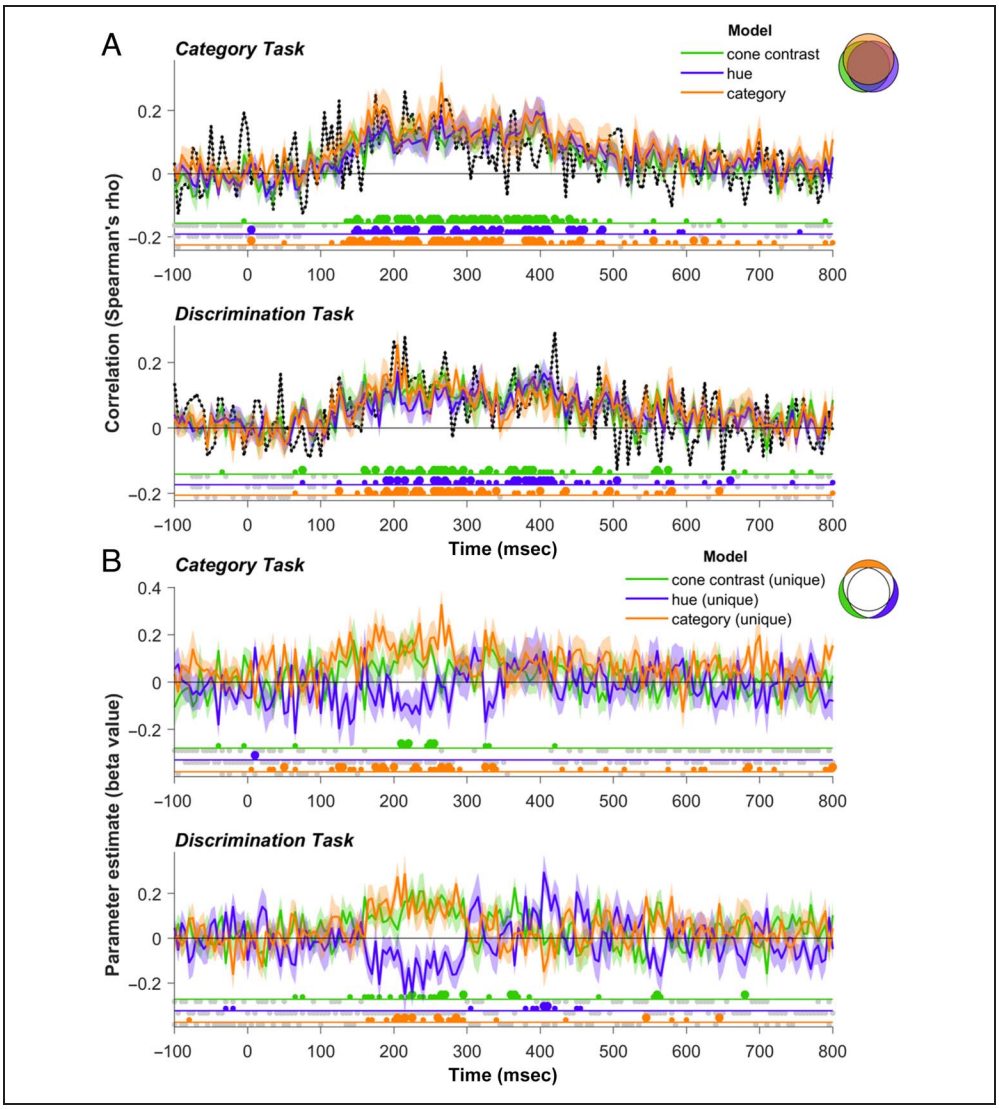

Figure 7. RSA. (A) Average correlations between individual participants' dissimilarity matrices for hue, and the cone contrast, hue and category models (see Figure 2 for models). (B) Parameter estimates from GLM, quantifying the unique variance captured by each model, beyond the variance shared by other models (see the Methods section for details). Colored regions of the Venn diagrams in the top right of A and B illustrate the variances captured by these different measures. In A, the lower bound of the noise ceiling (Nili et al., 2014; see the Methods section) is indicated by the dashed black line. Error bars are standard errors of the between-subject means, and dots below the *x* axis indicate the results of the Bayes Factor analysis, with plotting conventions as in Figure 4.

the stimulus-induced response. These correlations offer limited additional insight into the dynamics of color evident in the dissimilarity matrices and MDS solutions (Figure 6).

To better isolate the predictions of each model from the others and test whether the unique variance captured by each model varies over time, we used a GLM analysis (detailed in the methods), with results shown in Figure 7B. The cone contrast model, which we expected to perform best for the earliest cortical responses, accounted for some unique variance in the first half of the response, but this was not clearly restricted to the response onset for either task. Interestingly, although we initially included the "category" model to potentially capture later, higher-order color representations associated with color naming/categorization, we instead found that the unique variance captured by the category was most evident in the earlier part of the stimulus-induced response. This complements observations from the exploratory analysis (Figure 6) that the early color responses included clustering of some hues of the same category, most notably the greens. For data from the discrimination task, we also found that the hue model captured variance beyond that of the category model later in the response. This suggests that later in the response, representations of similar hues in the same color category are more distinct, reflecting their different appearance more than their category. This indication of a transition from the category to hue model better accounting for unique variance occurs at 300–350 msec after the stimulus onset, which is around the boundary between the second and third time windows in Figure 6. Together, these results suggest that the dynamic reorganization of color representations could include a transition from a coarse, early response, with greater clustering of hues of the same category, to a representation that accentuates the finer appearance differences between within-category hues.

Despite very similar overall patterns of effects, the GLM analyses (Figure 7B) also suggest some task-dependent effects, with the hue model accounting for unique variance at ~400 msec after stimulus onset when participants were performing the discrimination task, rather than the category task. The direction of this effect is consistent with the task requirements, because the discrimination task, but not the category task, required participants to pay attention to finer differences in hue, including within a color category.

DISCUSSION

In this article, we performed a series of classification analyses on the MEG recordings to explore how the neural response to color unfolds over time, using a combination of exploratory analyses (MDS) and hypothesis-driven RSA. We chose stimuli with a relatively fine sampling of the hue space (14 hue directions) with the aim of revealing distortions of the neural representation of color that could distinguish between different models of color representation.

The Importance of Comparing Multiple Models of Color Representation

In the RSA, we tested three different representations (models) of stimulus color, against the human cortical MEG data, with the aim of asking which model, if any, best captures the MEG-generated neural code. All models are based on human behavioral data. One representation of our chromatic stimuli is in a CIE L*a*b* space, where the 14 suprathreshold colors are equally spaced around a color circle in terms of their perceived color differences ("hue model"). In a second representation, these same stimuli are placed in a space based on the relative responses of the three different cone types to the stimuli ("cone contrast model"). In this space, stimuli vary in a nonuniform way although retaining the overall color stimulus ordering. The distortions in the cone contrast space reflect, at least in part, the differential contrast sensitivities of the two underlying cone opponent mechanisms, with the S-cone opponent direction elongated due to its poor contrast sensitivity compared with the highly sensitive L/M opponent mechanism (Sankeralli & Mullen, 1996; Cole, Hine, & McIlhagga, 1993). We selected a cone contrast model as it represents lower-level cortical responses in the visual system and provides a useful benchmark against which to compare other models. The simplest account of cortical color representations would be that they reflect their subcortical inputs, so a robust test of higher-level models is whether they account for color representations better than this lower-level one. The third color representation we tested is based on the categorical groupings of our 14 colors, measured individually for each participant's naming data, which produces a re-arrangement of the "hue model" stimuli into clusters, predicting high within-category similarity as well as an orderly progression of categories based on their hue similarity ("category model").

The Challenge of Overlapping Models

These three models are conceptually distinct and were selected as biologically plausible color spaces that may best capture the neural code. However, it is important to note that they are also correlated and so make substantially overlapping predictions in accounting for the observed data (e.g., the same ordering of hues). We overcome this issue by using the GLM analyses to compare the models in terms of the unique variance they capture (Figure 7B), which revealed differences between the three models to be seen that were invisible previously (Figure 7A). As mentioned above, comparing higher-level models with one based on a lower level of processing provides a valuable benchmark when considering what

constitutes evidence in favor of a higher-level model, and for both hue and category models, we find evidence that they significantly outperform the cone contrast model at different times.

Robust Decoding of Luminance and Hue

Across the stimulus-induced response, we found robust decoding of luminance and hue for both tasks, consistent with previous evidence that stimulus color can be decoded based on a topographic cortical representation of color in the MEG data (e.g., Goddard, Carlson, et al., 2022; Goddard, Shooner, et al., 2022; Hermann et al., 2022; Rosenthal et al., 2021; Teichmann et al., 2019, 2020). Decoding of both luminance and hue reached significance from approximately 100 msec after initial stimulus onset and is optimal between 200 and 400 msec. These onsets are slightly later than previously reported, and, unlike previous studies, we did not find evidence for decoding of luminance preceding that of hue (Hermann et al., 2022; Rosenthal et al., 2021). However, we note that our gradual onset stimuli may account for the later onset of the responses and are not optimized for comparing the onset of hue and luminance responses.

Patterns of luminance decoding (Figure 5) tended to indicate a neural representation based on luminance contrast, rather than luminance intensity. That is, accuracy was generally higher when the classifier was trained to discriminate between the isoluminant stimuli and those with luminance contrast, rather than between luminance increments and decrements, even though the latter have a greater difference in intensity. However, although decoding of luminance was highly robust, the pattern of decoding across luminance levels was variable across participants, and hence yielding only modest support for a neural representation based on luminance contrast rather than intensity.

Where in Cortex Are These Hue and Luminance Representations Located?

The spatial resolution of MEG source reconstruction does not allow us to make strong inferences about which visual cortical areas are contributing to the color representations. Although our source reconstruction indicated that sources were primarily located in visual cortex (Figure 3A–B), we found similar patterns of classifier results across early, ventral, and dorsal visual cortex (see the Appendix section). This could reflect dynamics that are propagating across these interconnected areas and/or that signals from these nearby regions were not well separated in our analyses. For this reason, the timing of the observed effects provides the clearest constraints on where these neural representations are located, which we consider below.

Orderly Hue Representations, with Minimal Differences across Task

RSA revealed hue representations that were less variable across participants than the luminance ones, possibly because our experimental design included larger variation in stimulus hue than luminance. From the onset of above-chance decoding, our data were consistent with all three of the models tested. This suggests that, from the earliest cortical responses to color, there is an orderly representation of hue. If the earliest stimulus-induced responses found here reflect the feedforward information in lower visual areas, and then our data differ from fMRI studies showing that the responses of areas such as V1 and V2 lack an orderly representation of hue, with orderly responses emerging only in higher areas such as hV4 and VO (Brouwer & Heeger, 2009). This discrepancy could be related to the fact that, in the fMRI study, participants' attention was diverted from the colored stimuli. Alternatively, it could be that any orderly representation of hue in V1 was relatively transient in the fMRI study and beyond the temporal resolution of fMRI. The data presented here are consistent with more recent evidence from optical imaging suggesting a "pinwheel" spatial organization of hue responses in V1 (Li et al., 2022).

The hue representations found here showed interesting temporal dynamics, considered below, but only modest variation with task. Using fMRI, Brouwer and Heeger (2013) demonstrated that areas hV4 and VO1 showed evidence of categorical clustering in hue representations, but this was present only when participants were engaged in a color naming task and not when their attention was diverted. We were interested in whether the categorical clustering reported by Brouwer and Heeger (2013) was specific to a task requiring categorization or a more general effect of attending to stimulus color. For this reason, we included a task requiring attention to color category (color-name 1-back task) as well as a task that required attention to color but without requiring categorization (exact-match 1-back task). The MDS and RSA analyses suggested that hue representations were largely consistent across the two tasks, but there was one noticeable trend in the RSA results in the direction of a task-specific effect, which we consider in the following section.

Dynamics of Hue Representations and a "Coarse to Fine" Transition

Our results show some interesting dynamics in the cortical response to color that are robust and replicated across data from both tasks. These dynamics are evident both in the MDS solutions (see Figure 6 or movies in the Appendix section) and in the GLM analyses (Figure 7B). The GLM analyses, key to comparing the different models, indicate that there is a reorganization of the representation of color at around 300–350 msec after stimulus onset. Before this time, the data tend to be

more consistent with the cone contrast model, potentially reflecting responses that modulate with cone contrast, and also with unique variance captured by the category model, supporting a representation based on a clustering of within-category hues. In the group data, this is seen in the MDS solutions primarily as a clustering of the neural responses to the green hues, although the dominance of the greens here may be driven by the fact that in our stimulus set, green was the largest category. After this reorganization, there is a more even separation of hues within the same category, as seen in the unique variance captured by the hue model in the latter part of the response for the discrimination task.

Inspection of the MDS solutions suggests that the neural data have systematic deviations from each of the three models we considered. Of course, it is possible that there are other color representations that would more closely match the observed data than the models we considered. Although we used the CIE L*a*b* space as an approximate model of color appearance in our "hue" model, there are numerous models of color appearance based on apparent color difference or discriminability (Fairchild, 2005), or on natural image statistics (Smet, Webster, & Whitehead, 2016), which would make similar predictions. However, given the substantial reorganization of these representations over time, it is unlikely that there is any single (static) model that could capture the neural representational space across time. For instance, our "hue" model may not be an accurate model of perceptual difference, because although CIE L*a*b* space is designed to be approximately perceptually uniform, it contains known deviations from a truly Euclidian space (Ennis & Zaidi, 2019). However, we find more pronounced deviations from the model based on CIE L*a*b* space than predicted by these known nonlinearities, and more importantly, the MDS results suggest that the neural data deviate from the CIE L*a*b* space in different ways over time: Although greens are initially more clustered together than predicted by the hue model, at later times, they are relatively more separated than other hues. Overall, the most pronounced feature of the hue representations in our data is their dynamic reorganization over time.

It is interesting that the category model performs best in the earlier part of the neural response. Because higher-level areas like hV4 and VO are associated with higher-level responses to color, including categorical representations (Brouwer & Heeger, 2013), we might expect that any categorical effects would emerge later in the stimulus-induced response, possibly incorporating feedback effects related to task and/or language. Instead, we found early contributions of the category model, meaning it is very unlikely that these reflect a higher-level representation where hues of the same semantic label are coded in a more similar way than hues of different names. Instead, we interpret these findings as suggesting that, during earliest cortical responses, there are hues that evoke very similar responses, which are then differentiated later in the response, but that this early clustering is not related to the influence of language. The "earlier" timeframe of the categorial model includes responses from response onset, likely driven by areas such as V1 and V2, up to 300 msec after stimulus onset, by which time the data would also include responses from higher-order areas such as hV4 and VO, and more anterior color centers (Lafer-Sousa et al., 2016; Zeki & Bartels, 1999). For instance, subdural electrode recordings in human VVC, anterior to hV4, showed neuronal responses to color from ~100 msec after stimulus onset, peaking at ~150 msec after stimulus onset (Murphey, Yoshor, & Beauchamp, 2008).

After ~300 msec post stimulus onset, there is no evidence of increasing categorical clustering. Hence, our data argue against the idea that any feedback or recurrent processing within cortex is driving hue representations to become more categorical over time. Instead, we find that hue representations of finer, within-category differences become stronger over time. This transition may echo the "coarse to fine" strategy in different aspects of spatial vision, with the coarse color structure processed before the fine within-color detail. Although coarse-to-fine processing typically refers to neural responses shifting from lower to higher spatial scale information over time (e.g., Goffaux et al., 2011; Watt, 1987), equivalent coding principles have been implicated in orientation coding (Ringach, Hawken, & Shapley, 1997, 2003; Shapley, Hawken, & Ringach, 2003) and face processing (Dobs, Isik, Pantazis, & Kanwisher, 2019), where initial responses are more coarsely tuned, preceding representations of finer differences (i.e., wider then narrower tuning for orientation responses, face age, and gender preceding representations that differentiate between face identities).

The late time at which we observe this transition to an enhanced representation of finer hue differences (~300 msec) suggests that these effects could be at least partly driven by top–down effects of attention, which have previously been reported to produced effects consistent with sharpening of population tuning for color (Goddard, Carlson, et al., 2022; Bartsch et al., 2017). In both conditions, participants were attending to color, and across both tasks, we saw similar dynamics, consistent with a transition from coarser to finer hue representations. However, at later stages of the stimulus-induced response, there was stronger evidence in favor of the hue model for data from the discrimination task than for the category task at corresponding times (Figure 7B). This task-specific effect is much subtler than the fMRI differences when comparing a categorical task with diverted attention (Brouwer & Heeger, 2013), suggesting that the effect of attending to a colored stimulus, rather than specifically attending to its category, is of greater relevance.

A final notable feature of the hue representations in our data is in the latter part of the neural response (e.g., the 340- to 455-msec and 455- to 570-msec time windows in Figure 6); the hue closest to yellow is also close to one or more blue hues. This is clearest in the

MDS results in the 340- to 455-msec time window, where the hue circle is represented more as a "figure of 8," with crossing at yellow/blue, but within greenish and reddish hues, there is greater separation. This is not accounted for by the S-cone inputs being slower to reach cortex than red-green signals carried by the parvocellular pathway (e.g., Cottaris & De Valois, 1998), because the effect we observe is well after the initial cortical response and because the effect is in the opposite direction, with a relatively late encoding of red-green differences. Although these observations are still speculative and based on an exploratory analysis, we note that in both tasks, the yellow/blue crossing occurred not for the extremes along the S-cone isolating axis but closer to unique yellow/blue and the daylight axis (Delahunt & Brainard, 2004). We did not design this work to test for such asymmetries, but these observations could motivate future work to characterize these.

Conclusion

In summary, in this MEG study, we reveal a dynamic reorganization of the cortical response to color over time, which is remarkably consistent across our two tasks. We compared three conceptually distinct, biologically plausible models that may best capture the neural code, using GLM analyses to isolate the unique data variance accounted for by each model. The resulting model dynamics reflects a "coarse to fine" transition over time from an early categorial grouping of colors in the cortical representation evolving into a finer, more even separation of the hues.

APPENDIX

This appendix includes figures equivalent to those in the main text but for other ROIs (VVC, dorsal visual cortex, DVC), in Figures A1–A8.

Directly below, we include a description of the videos included in this appendix as separate files, which may be downloaded on the article of the webpage: https://doi.org/10.1162/jocn.a.56.

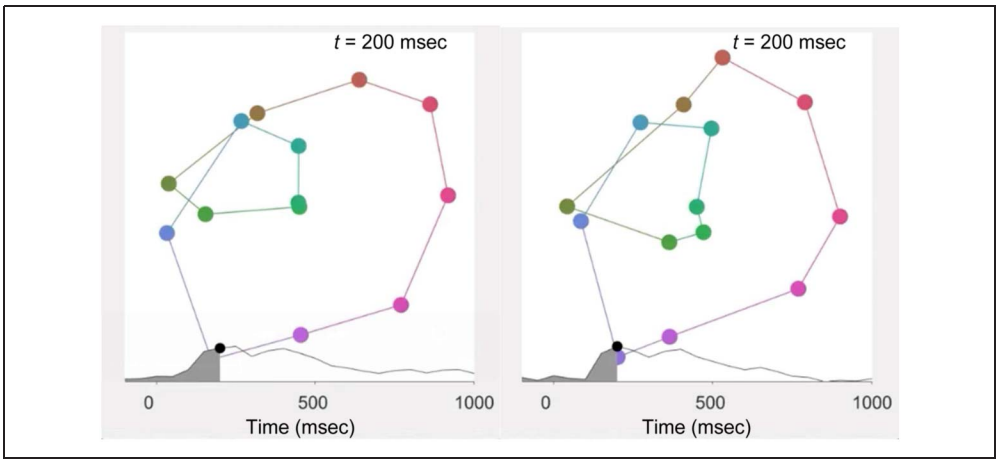

Videos A1–A2. Videos of MDS solutions for data from the category task (left) and discrimination task (right) over time (−100 to 1000 msec, 50-msec bins), based on classifier. Performance in the EVC (n = 8). These are still frames from the videos, which are included in the Appendix as separate files.

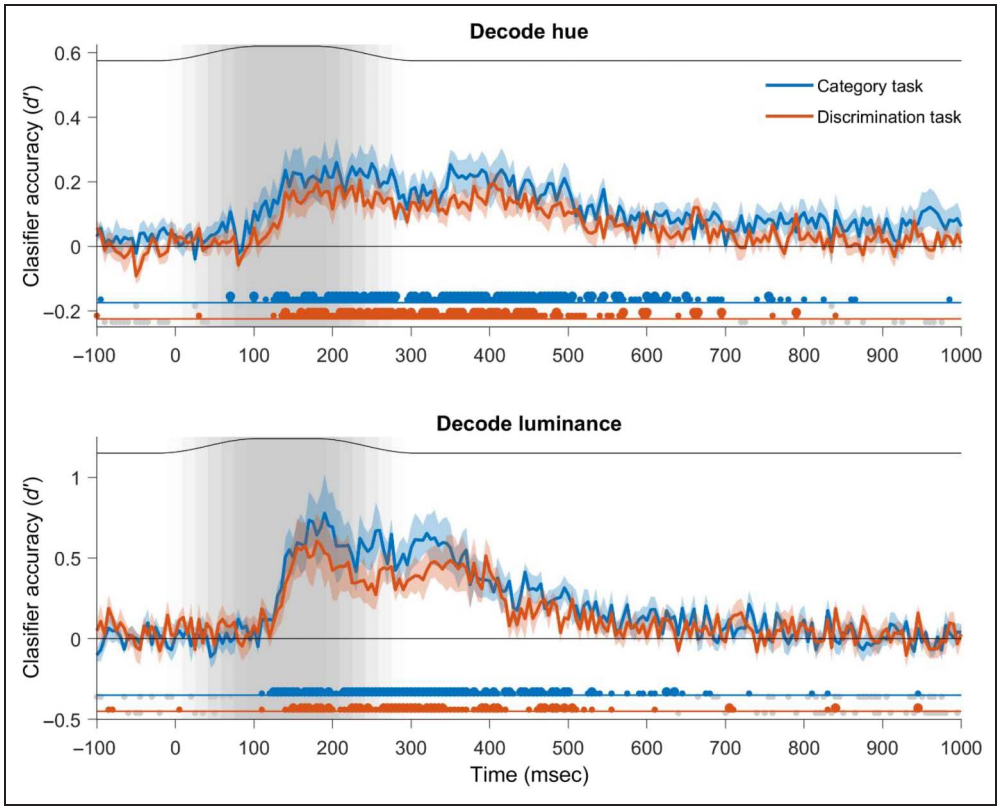

Figure A1. Decoding of stimulus hue (upper) and luminance (lower) for classifiers trained on data from the VVC. Plotting conventions as in Figure 4.

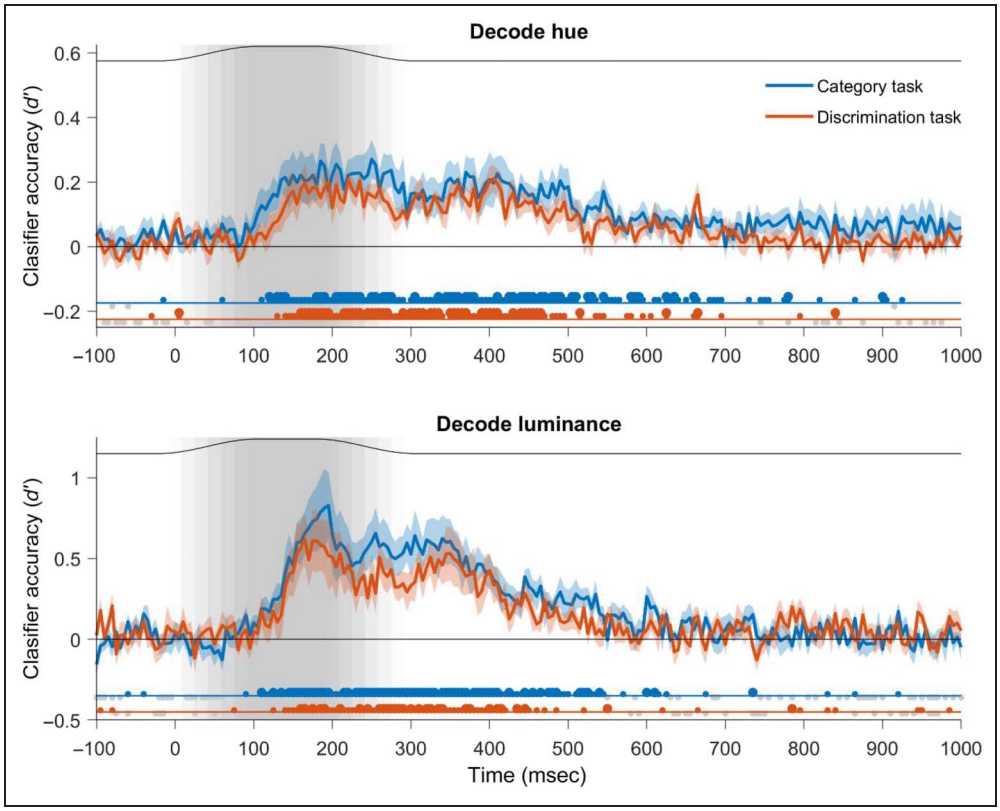

Figure A2. Decoding of stimulus hue (upper) and luminance (lower) for classifiers trained on data from the DVC. Plotting conventions as in Figure 4.

Figure A3. RSA of stimulus luminance, for the category (upper) and discrimination (lower) tasks for classifiers trained on data from the VVC. Plotting conventions as in Figure 5.

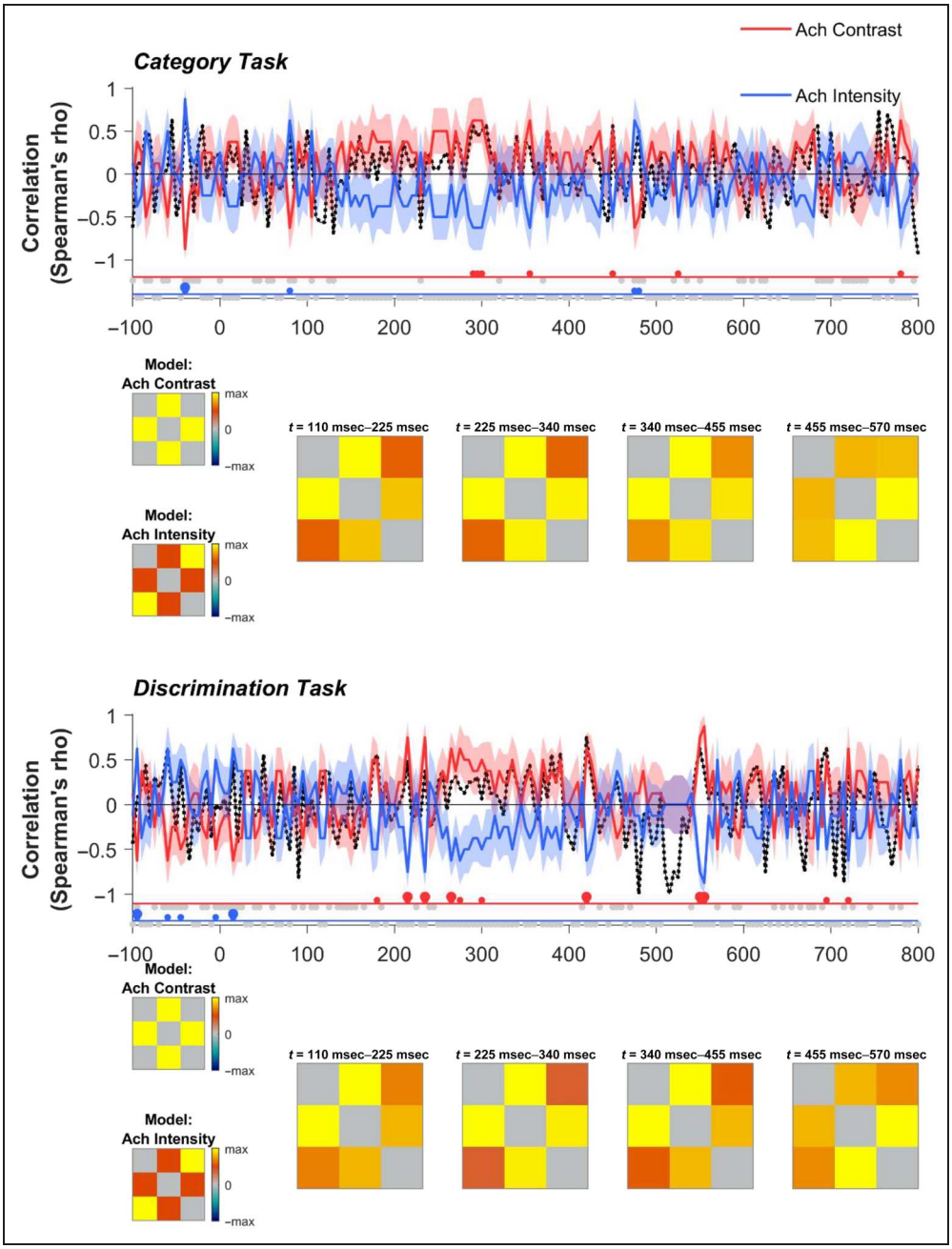

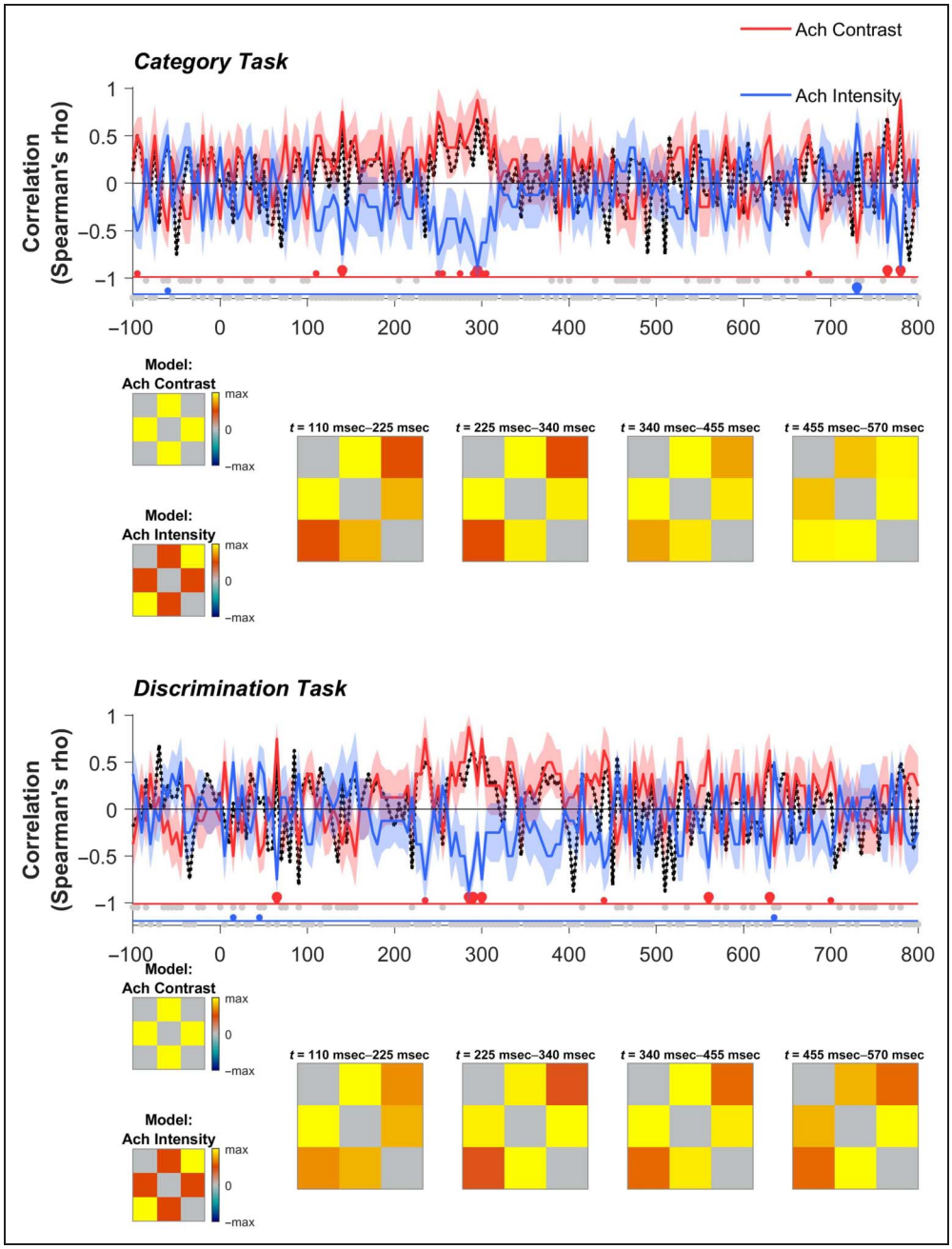

Figure A4. RSA of stimulus luminance, for the category (upper) and discrimination (lower) tasks for classifiers trained on data from the DVC. Plotting conventions as in Figure 5.

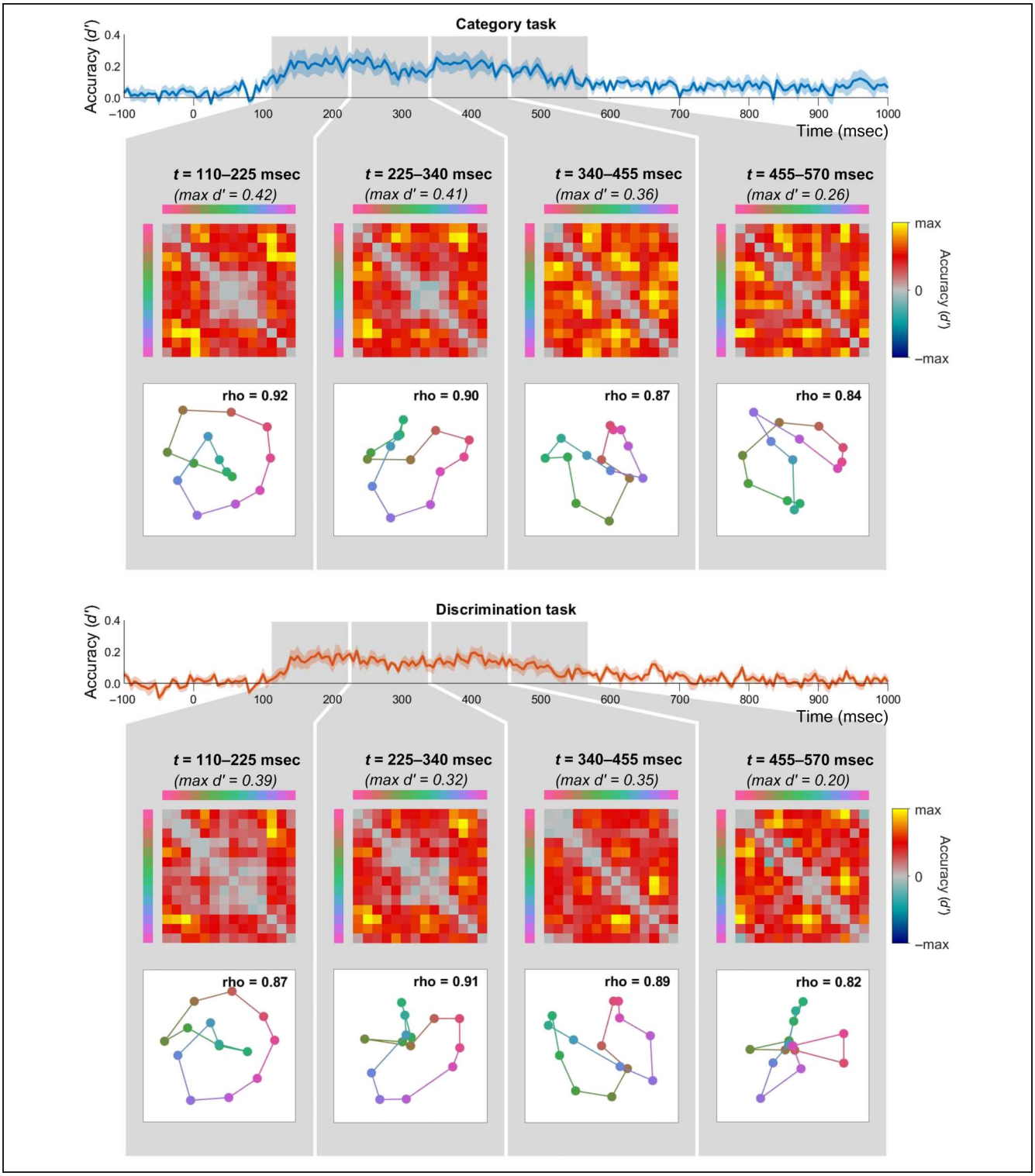

Figure A5. Average DSMs and corresponding MDS solutions for data from the category task (upper) and discrimination task (lower) for classifiers trained on data from the VVC. Plotting conventions as in Figure 6.

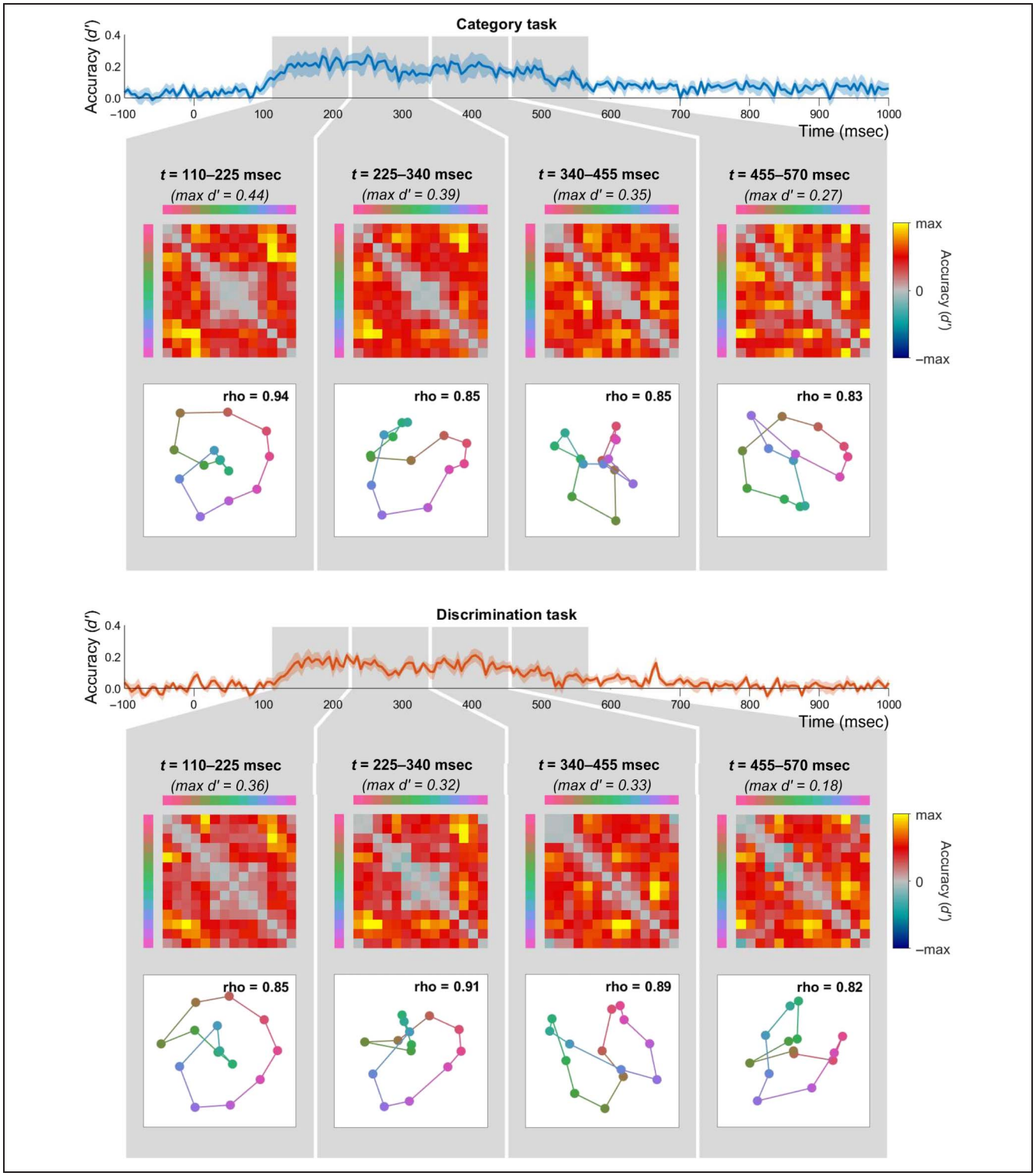

Figure A6. Average DSMs and corresponding MDS solutions for data from the category task (upper) and discrimination task (lower) for classifiers trained on data from the DVC. Plotting conventions as in Figure 6.

Figure A7. RSA of hue decoding, for classifiers trained on data from the VVC. Plotting conventions as in Figure 7.

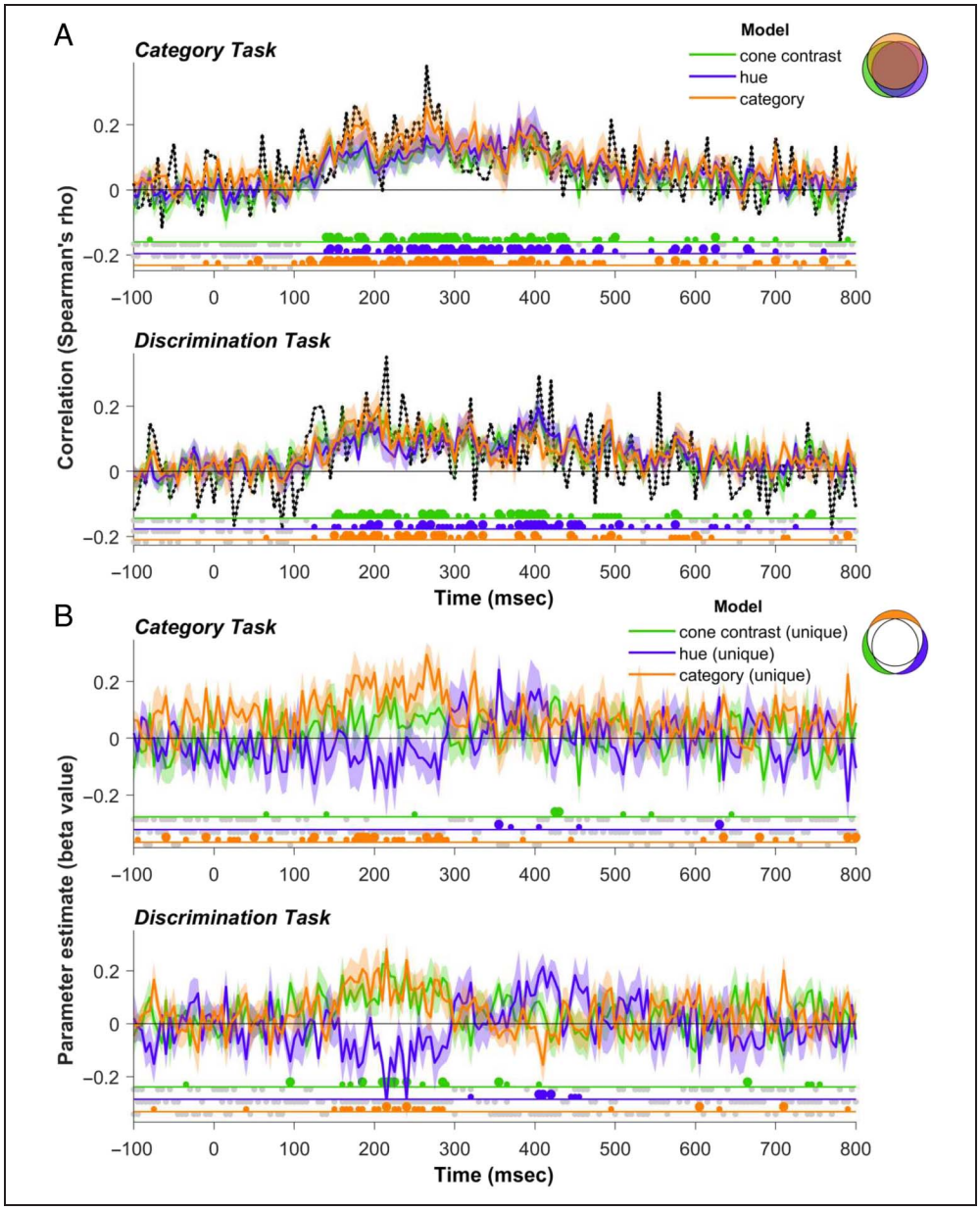

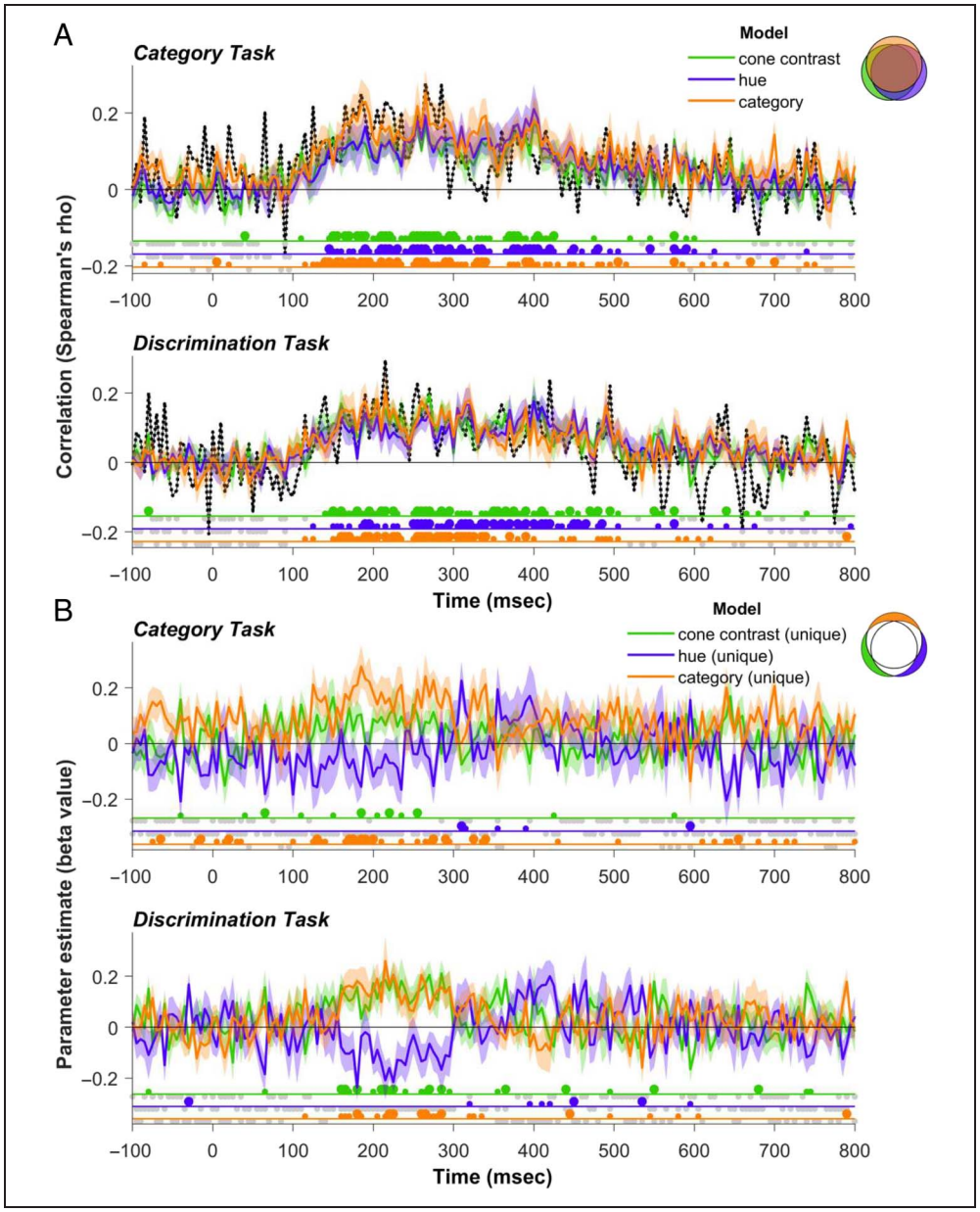

Figure A8. RSA of hue decoding, for classifiers trained on data from the DVC. Plotting conventions as in Figure 7.

Corresponding author: Kathy T. Mullen, McGill Vision Research, Department of Ophthalmology & Visual Sciences, McGill University, Montreal, QC, H3G1A4, Canada, e-mail: kathy.mullen@mcgill.ca.

Data Availability Statement

Data from MEG experiments are freely available online from the Open Science Framework (https://doi.org/10.17605/OSF.IO/KMFZ7). This online repository includes deidentified MEG data from the MEG experiments and details of the stimulus timing for each participant.

Author Contributions

Erin Goddard: Conceptualization; Data curation; Formal analysis; Investigation; Visualization; Writing—Original draft; Writing—Review & editing. Kathy T. Mullen: Conceptualization; Funding acquisition; Writing—Original draft; Writing—Review & editing.

Funding Information

This work was funded by Canadian Institutes of Health Research (https://dx.doi.org/10.13039/501100000024; CIHR) grants 153277 and 10819 and Natural Science and Engineering Research Council of Canada (NSERC) grant RGPIN 03824 to K. T. M. E. G. was partly supported by the Australian Research Council (https://dx.doi.org/10.13039/501100000923; DP220100747). We thank Christopher Shooner for help with the design and data collection, and we thank Marc Lalancette for advice on MEG protocols. We thank all our participants for their assistance with data collection.

Diversity in Citation Practices

Retrospective analysis of the citations in every article published in this journal from 2010 to 2021 reveals a persistent pattern of gender imbalance: Although the proportions of authorship teams (categorized by estimated gender identification of first author/last author) publishing in the *Journal of Cognitive Neuroscience* (*JoCN*) during this period were M(an)/M = .407, W(oman)/M = .32, M/W = .115, and W/W = .159, the comparable proportions for the articles that these authorship teams cited were M/M = .549, W/M = .257, M/W = .109, and W/W = .085 (Postle and Fulvio, *JoCN*, 34:1, pp. 1–3). Consequently, *JoCN* encourages all authors to consider gender balance explicitly when selecting which articles to cite and gives them the opportunity to report their article's gender citation balance. The authors of this article report its proportions of citations by gender category to be: M/M = .477; W/M = .205; M/W = .045; W/W = .273.

REFERENCES

Bae, G.-Y., & Chen, K.-W. (2024). EEG decoding reveals task-dependent recoding of sensory information in working memory. *Neuroimage*, *297*, 120710. https://doi.org/10.1016/j.neuroimage.2024.120710, PubMed: 38942100

Bartsch, M. V., Loewe, K., Merkel, C., Heinze, H.-J., Schoenfeld, M. A., Tsotsos, J. K., et al. (2017). Attention to color sharpens neural population tuning via feedback processing in the human visual cortex hierarchy. *Journal of Neuroscience*, *37*, 10346–10357. https://doi.org/10.1523/JNEUROSCI.0666-17.2017, PubMed: 28947573

Berlin, B., & Kay, P. (1969). *Basic color terms: Their universality and evolution*. University of California Press.

Brainard, D. H. (1997). The psychophysics toolbox. *Spatial Vision*, *10*, 433–436. PubMed: 9176952

Brewer, A. A., Liu, J., Wade, A. R., & Wandell, B. A. (2005). Visual field maps and stimulus selectivity in human ventral occipital cortex. *Nature Neuroscience*, *8*, 1102–1109. https://doi.org/10.1038/nn1507, PubMed: 16025108

Brouwer, G. J., & Heeger, D. J. (2009). Decoding and reconstructing color from responses in human visual cortex. *Journal of Neuroscience*, *29*, 13992–14003. https://doi.org/10.1523/JNEUROSCI.3577-09.2009, PubMed: 19890009

Brouwer, G. J., & Heeger, D. J. (2013). Categorical clustering of the neural representation of color. *Journal of Neuroscience*, *33*, 15454–15465. https://doi.org/10.1523/JNEUROSCI.2472-13.2013, PubMed: 24068814

Chauhan, T., Jakovljev, I., Thompson, L. N., Wuerger, S. M., & Martinovic, J. (2023). Decoding of EEG signals reveals non-uniformities in the neural geometry of colour. *Neuroimage*, *268*, 119884. https://doi.org/10.1016/j.neuroimage.2023.119884, PubMed: 36657691

Cole, G. R., Hine, T., & McIlhagga, W. (1993). Detection mechanisms in L-, M-, and S-cone contrast space. *Journal of the Optical Society of America A*, *10*, 38–51. https://doi.org/10.1364/JOSAA.10.000038, PubMed: 8478744

Conway, B. R., Malik-Moraleda, S., & Gibson, E. (2023). Color appearance and the end of Hering's Opponent-Colors Theory. *Trends in Cognitive Sciences*, *27*, 791–804. https://doi.org/10.1016/j.tics.2023.06.003, PubMed: 37394292

Cottaris, N. P., & De Valois, R. L. (1998). Temporal dynamics of chromatic tuning in macaque primary visual cortex. *Nature*, *395*, 896–900. https://doi.org/10.1038/27666, PubMed: 9804422

Dale, A. M., Fischl, B., & Sereno, M. I. (1999). Cortical surface-based analysis. I. Segmentation and surface reconstruction. *Neuroimage*, *9*, 179–194. https://doi.org/10.1006/nimg.1998.0395, PubMed: 9931268

Delahunt, P. B., & Brainard, D. H. (2004). Does human color constancy incorporate the statistical regularity of natural daylight? *Journal of Vision*, *4*, 57–81. https://doi.org/10.1167/4.2.1, PubMed: 15005648

Derrington, A. M., Krauskopf, J., & Lennie, P. (1984). Chromatic mechanisms in lateral geniculate nucleus of macaque. *Journal of Physiology*, *357*, 241–265. https://doi.org/10.1113/jphysiol.1984.sp015499, PubMed: 6512691

De Valois, R. L., & De Valois, K. K. (1993). A multi-stage color model. *Vision Research*, *33*, 1053–1065. https://doi.org/10.1016/0042-6989(93)90240-W, PubMed: 8506645

Dobs, K., Isik, L., Pantazis, D., & Kanwisher, N. (2019). How face perception unfolds over time. *Nature Communications*, *10*, 1258. https://doi.org/10.1038/s41467-019-09239-1, PubMed: 30890707

Engel, S. A., Rumelhart, D. E., Wandell, B. A., Lee, A. T., Glover, G. H., Chichilnisky, E. J., et al. (1994). fMRI of human visual cortex. *Nature*, *369*, 525. https://doi.org/10.1038/369525a0, PubMed: 80314303

Ennis, R. J., & Zaidi, Q. (2019). Geometrical structure of perceptual color space: Mental representations and adaptation invariance. *Journal of Vision*, *19*, 1. https://doi.org/10.1167/19.12.1, PubMed: 31573606

Eskew, R. T., Jr. (2009). Higher order color mechanisms: A critical review. *Vision Research*, *49*, 2686–2704. https://doi.org/10.1016/j.visres.2009.07.005, PubMed: 19616020

Fairchild, M. D. (2005). *Color appearance models*. John Wiley & Sons, Inc.

Farnsworth, D. (1957). *The Farnsworth-Munsell 100-hue test for the examination of color discrimination*. Macbeth, a division of Kollmorgen Corp.

Fischl, B., Sereno, M. I., & Dale, A. M. (1999). Cortical surface-based analysis. II: Inflation, flattening, and a surface-based coordinate system. *Neuroimage*, *9*, 195–207. https://doi.org/10.1006/nimg.1998.0396, PubMed: 9931269

Goddard, E., Carlson, T. A., & Woolgar, A. (2022). Spatial and feature-selective attention have distinct, interacting effects on population-level tuning. *Journal of Cognitive Neuroscience*, *34*, 290–312. https://doi.org/10.1162/jocn_a_01796, PubMed: 34813647

Goddard, E., Chang, D. H. F., Hess, R. F., & Mullen, K. T. (2019). Color contrast adaptation: fMRI fails to predict behavioral adaptation. *Neuroimage*, *201*, 116032. https://doi.org/10.1016/j.neuroimage.2019.116032, PubMed: 31326574

Goddard, E., Mannion, D. J., McDonald, J. S., Solomon, S. G., & Clifford, C. W. G. (2011). Color responsiveness argues against a dorsal component of human V4. *Journal of Vision*, *11*, 3. https://doi.org/10.1167/11.4.3, PubMed: 21467155

Goddard, E., Mannion, D. M., McDonald, J. S., Solomon, S. G., & Clifford, C. W. G. (2010). Combination of subcortical color channels in human visual cortex. *Journal of Vision*, *10*, 25. https://doi.org/10.1167/10.5.25, PubMed: 20616126

Goddard, E., & Mullen, K. T. (2020). fMRI representational similarity analysis reveals graded preferences for chromatic and achromatic stimulus contrast across human visual cortex. *Neuroimage*, *215*, 116780. https://doi.org/10.1016/j.neuroimage.2020.116780, PubMed: 32276074

Goddard, E., & Mullen, K. T. (2021). Attention selectively enhances stimulus information for surround over foveal stimulus representations in occipital cortex. *Journal of Vision*, *21*, 20. https://doi.org/10.1167/jov.21.3.20, PubMed: 33749755

Goddard, E., Shooner, C., & Mullen, K. T. (2022). Magnetoencephalography contrast adaptation reflects perceptual adaptation. *Journal of Vision*, *22*, 16. https://doi.org/10.1167/jov.22.10.16, PubMed: 36121660

Goffaux, V., Peters, J., Haubrechts, J., Schiltz, C., Jansma, B., & Goebel, R. (2011). From coarse to fine? Spatial and temporal dynamics of cortical face processing. *Cerebral Cortex*, *21*, 467–476. https://doi.org/10.1093/cercor/bhq112, PubMed: 20576927

Golub, G. H., & Loan, C. F. V. (1996). *Matrix computations, third edition*. Johns Hopkins University Press.

Grootswagers, T., Robinson, A. K., Shatek, S. M., & Carlson, T. A. (2024). Mapping the dynamics of visual feature coding: Insights into perception and integration. *PLoS Computational Biology*, *20*, e1011760. https://doi.org/10.1371/journal.pcbi.1011760, PubMed: 38190390

Hajonides, J. E., Nobre, A. C., van Ede, F., & Stokes, M. G. (2021). Decoding visual colour from scalp electroencephalography measurements. *Neuroimage*, 118030. https://doi.org/10.1016/j.neuroimage.2021.118030, PubMed: 33836272

He, J., Taveras Cruz, Y., & Eskew, R. T., Jr. (2020). Methods for determining equiluminance in terms of L/M cone ratios. *Journal of Vision*, *20*, 22. https://doi.org/10.1167/jov.20.4.22, PubMed: 32343780

Hermann, K. L., Singh, S. R., Rosenthal, I. A., Pantazis, D., & Conway, B. R. (2022). Temporal dynamics of the neural representation of hue and luminance polarity. *Nature Communications*, *13*, 661. https://doi.org/10.1038/s41467-022-28249-0, PubMed: 35115511

Huang, M. X., Mosher, J. C., & Leahy, R. M. (1999). A sensor-weighted overlapping-sphere head model and exhaustive head model comparison for MEG. *Physics in Medicine and Biology*, *44*, 423–440. https://doi.org/10.1088/0031-9155/44/2/010, PubMed: 10070792

Huk, A. C., Dougherty, R. F., & Heeger, D. J. (2002). Retinotopy and functional subdivision of human areas MT and MST. *Journal of Neuroscience*, *22*, 7195–7205. https://doi.org/10.1523/JNEUROSCI.22-16-07195.2002, PubMed: 12177214

Ishihara, S. (1990). *Ishihara's tests for color-blindness, 38 plate ed*. Kanehara, Shuppan Co. Ltd.

Kass, R. E., & Raftery, A. E. (1995). Bayes factors. *Journal of the American Statistical Association*, *90*, 773–795. https://doi.org/10.1080/01621459.1995.10476572

Kleiner, M., Brainard, D., & Pelli, D. G. (2007). What's new in psychtoolbox-3? *Perception*, *36*, 1–16.

Komatsu, H., Ideura, Y., Kaji, S., & Yamane, S. (1992). Color selectivity of neurons in the inferior temporal cortex of the awake macaque monkey. *Journal of Neuroscience*, *12*, 408–424. https://doi.org/10.1523/JNEUROSCI.12-02-00408.1992, PubMed: 1740688

Krekelberg, B. (2021). *klabhub/bayesFactor: Ttest updates* (Version v2.2.0) [Computer software]. Zenodo. https://doi.org/10.5281/zenodo.5707551

Kriegeskorte, N., Mur, M., & Bandettini, P. (2008). Representational similarity analysis—Connecting the branches of systems neuroscience. *Frontiers in Systems Neuroscience*, *2*, 4. https://doi.org/10.3389/neuro.06.004.2008, PubMed: 19104670

Kriegeskorte, N., Mur, M., Ruff, D. A., Kiani, R., Bodurka, J., Esteky, H., et al. (2008). Matching categorical object representations in inferior temporal cortex of man and monkey. *Neuron*, *60*, 1126–1141. https://doi.org/10.1016/j.neuron.2008.10.043, PubMed: 19109916

Lafer-Sousa, R., & Conway, B. R. (2013). Parallel, multi-stage processing of colors, faces and shapes in macaque inferior temporal cortex. *Nature Neuroscience*, *16*, 1870–1878. https://doi.org/10.1038/nn.3555, PubMed: 24141314

Lafer-Sousa, R., Conway, B. R., & Kanwisher, N. G. (2016). Color-biased regions of the ventral visual pathway lie between face- and place-selective regions in humans, as in macaques. *Journal of Neuroscience*, *36*, 1682–1697. https://doi.org/10.1523/JNEUROSCI.3164-15.2016, PubMed: 26843649

Larsson, J., & Heeger, D. J. (2006). Two retinotopic visual areas in human lateral occipital cortex. *Journal of Neuroscience*, *26*, 13128–13142. https://doi.org/10.1523/JNEUROSCI.1657-06.2006, PubMed: 17182764

Lennie, P., & Movshon, J. A. (2005). Coding of color and form in the geniculostriate visual pathway. *Journal of the Optical Society of America A*, *22*, 2013–2033. https://doi.org/10.1364/JOSAA.22.002013, PubMed: 16277273

Li, P., Garg, A. K., Zhang, L. A., Rashid, M. S., & Callaway, E. M. (2022). Cone opponent functional domains in primary visual cortex combine signals for color appearance mechanisms. *Nature Communications*, *13*, 6344. https://doi.org/10.1038/s41467-022-34020-2, PubMed: 36284139

Michna, M. L., Yoshizawa, T., & Mullen, K. T. (2007). S-cone contributions to linear and non-linear motion processing. *Vision Research*, *47*, 1042–1054. https://doi.org/10.1016/j.visres.2007.01.014, PubMed: 17343890

Morey, R. D., & Wagenmakers, E.-J. (2014). Simple relation between Bayesian order-restricted and point-null hypothesis tests. *Statistics & Probability Letters*, *92*, 121–124. https://doi.org/10.1016/j.spl.2014.05.010

Mullen, K. T., Dumoulin, S. O., & Hess, R. F. (2008). Color responses of the human lateral geniculate nucleus: [Corrected] selective amplification of S-cone signals between the lateral geniculate nucleno and primary visual cortex measured with high-field fMRI. *European Journal of Neuroscience*, *28*, 1911–1923. https://doi.org/10.1111/j.1460-9568.2008.06476.x, PubMed: 18973604

Mullen, K. T., Dumoulin, S. O., McMahon, K. L., de Zubicaray, G. I., & Hess, R. F. (2007). Selectivity of human retinotopic visual cortex to S-cone-opponent, L/M-cone-opponent and achromatic stimulation. *European Journal of Neuroscience*, *25*, 491–502. https://doi.org/10.1111/j.1460-9568.2007.05302.x, PubMed: 17284191

Mullen, K. T., & Sankeralli, M. J. (1999). Evidence for the stochastic independence of the blue-yellow, red-green and luminance detection mechanisms revealed by subthreshold summation. *Vision Research*, *39*, 733–745. https://doi.org/10.1016/S0042-6989(98)00137-0, PubMed: 10341960

Murphey, D. K., Yoshor, D., & Beauchamp, M. S. (2008). Perception matches selectivity in the human anterior color center. *Current Biology*, *18*, 216–220. https://doi.org/10.1016/j.cub.2008.01.013, PubMed: 18258428

Nili, H., Wingfield, C., Walther, A., Su, L., Marslen-Wilson, W., & Kriegeskorte, N. (2014). A toolbox for representational similarity analysis. *PLoS Computational Biology*, *10*, e1003553. https://doi.org/10.1371/journal.pcbi.1003553, PubMed: 24743308

Parkes, L. M., Marsman, J.-B. C., Oxley, D. C., Goulermas, J. Y., & Wuerger, S. M. (2009). Multivoxel fMRI analysis of color tuning in human primary visual cortex. *Journal of Vision*, *9*, 1.1–1.13. https://doi.org/10.1167/9.1.1, PubMed: 19271871

Pelli, D. G. (1997). The VideoToolbox software for visual psychophysics: Transforming numbers into movies. *Spatial Vision*, *10*, 437–442. https://doi.org/10.1163/156856897X00366, PubMed: 9176953

Popal, H., Wang, Y., & Olson, I. R. (2019). A guide to representational similarity analysis for social neuroscience. *Social Cognitive and Affective Neuroscience*, *14*, 1243–1253. https://doi.org/10.1093/scan/nsz099, PubMed: 31989169

Retter, T. L., Gao, Y., Jiang, F., Rossion, B., & Webster, M. A. (2023). Automatic, early color-specific neural responses to

object color knowledge. *Brain Topography*, *36*, 710–726. https://doi.org/10.1007/s10548-023-00979-4, PubMed: 37382839
Ringach, D. L., Hawken, M. J., & Shapley, R. (1997). Dynamics of orientation tuning in macaque primary visual cortex. *Nature*, *387*, 281–284. https://doi.org/10.1038/387281a0, PubMed: 9153392
Ringach, D. L., Hawken, M. J., & Shapley, R. (2003). Dynamics of orientation tuning in macaque V1: The role of global and tuned suppression. *Journal of Neurophysiology*, *90*, 342–352. https://doi.org/10.1152/jn.01018.2002, PubMed: 12611936
Rosenthal, I. A., Singh, S. R., Hermann, K. L., Pantazis, D., & Conway, B. R. (2021). Color space geometry uncovered with magnetoencephalography. *Current Biology*, *31*, 515–526. https://doi.org/10.1016/j.cub.2020.10.062, PubMed: 33202253
Rozman, A., Chauhan, T., & Martinovic, J. (2024). *Characterising representations of hue and saturation in the cortex using information decoding* (p. 2024.12.19.628842). bioRxiv. https://doi.org/10.1101/2024.12.19.628842
Sandhaeger, F., von Nicolai, C., Miller, E. K., & Siegel, M. (2019). Monkey EEG links neuronal color and motion information across species and scales. *eLife*, *8*, e45645. https://doi.org/10.7554/eLife.45645, PubMed: 31287792
Sankeralli, M. J., & Mullen, K. T. (1996). Estimation of the L-, M-, and S-cone weights of the postreceptoral detection mechanisms. *Journal of the Optical Society of America A*, *13*, 906–915. https://doi.org/10.1364/JOSAA.13.000906
Schira, M. M., Tyler, C. W., Breakspear, M., & Spehar, B. (2009). The foveal confluence in human visual cortex. *Journal of Neuroscience*, *29*, 9050–9058. https://doi.org/10.1523/JNEUROSCI.1760-09.2009, PubMed: 19605642
Sereno, M. I., Dale, A. M., Reppas, J. B., Kwong, K. K., Belliveau, J. W., Brady, T. J., et al. (1995). Borders of multiple visual areas in humans revealed by functional magnetic resonance imaging. *Science*, *268*, 889–893. https://doi.org/10.1126/science.7754376, PubMed: 7754376
Shapley, R., Hawken, M., & Ringach, D. L. (2003). Dynamics of orientation selectivity in the primary visual cortex and the importance of cortical inhibition. *Neuron*, *38*, 689–699. https://doi.org/10.1016/S0896-6273(03)00332-5, PubMed: 12797955
Siuda-Krzywicka, K., Boros, M., Bartolomeo, P., & Witzel, C. (2019). The biological bases of colour categorisation: From goldfish to the human brain. *Cortex*, *118*, 82–106. https://doi.org/10.1016/j.cortex.2019.04.010, PubMed: 31151746
Smet, K. A. G., Webster, M. A., & Whitehead, L. A. (2016). A simple principled approach for modeling and understanding uniform color metrics. *Journal of the Optical Society of America A*, *33*, A319–A331. https://doi.org/10.1364/JOSAA.33.00A319, PubMed: 26974939
Smith, V. C., & Pokorny, J. (1975). Spectral sensitivity of the foveal cone photopigments between 400 and 500 nm. *Vision Research*, *15*, 161–171. https://doi.org/10.1016/0042-6989(75)90203-5, PubMed: 1129973
Stockman, A., & Brainard, D. H. (2010). Color vision mechanisms. In M. Bass (Ed.), *Handbook of optics: Volume III - vision and vision optics* (3rd Edition). McGraw-Hill Education. https://www.accessengineeringlibrary.com/content/book/9780071498913/chapter/chapter11
Stoughton, C. M., & Conway, B. R. (2008). Neural basis for unique hues. *Current Biology*, *18*, R698–R699. https://doi.org/10.1016/j.cub.2008.06.018, PubMed: 18727902
Sutterer, D. W., Coia, A. J., Sun, V., Shevell, S. K., & Awh, E. (2021). Decoding chromaticity and luminance from patterns of EEG activity. *Psychophysiology*, *58*, e13779. https://doi.org/10.1111/psyp.13779, PubMed: 33550667
Tadel, F., Baillet, S., Mosher, J. C., Pantazis, D., & Leahy, R. M. (2011). Brainstorm: A user-friendly application for MEG/EEG analysis. *Computational Intelligence and Neuroscience*, *2011*, 879716. https://doi.org/10.1155/2011/879716, PubMed: 21584256
Teichmann, L., Grootswagers, T., Carlson, T. A., & Rich, A. N. (2019). Seeing versus knowing: The temporal dynamics of real and implied colour processing in the human brain. *Neuroimage*, *200*, 373–381. https://doi.org/10.1016/j.neuroimage.2019.06.062, PubMed: 31254648
Teichmann, L., Moerel, D., Baker, C., & Grootswagers, T. (2022). An empirically driven guide on using Bayes factors for M/EEG decoding. *Aperture Neuro*, *2*, 1–10. https://doi.org/10.52294/ApertureNeuro.2022.2.MAOC6465
Teichmann, L., Quek, G. L., Robinson, A. K., Grootswagers, T., Carlson, T. A., & Rich, A. N. (2020). The influence of object-color knowledge on emerging object representations in the brain. *Journal of Neuroscience*, *40*, 6779–6789. https://doi.org/10.1523/JNEUROSCI.0158-20.2020, PubMed: 32703903
Uusitalo, M. A., & Ilmoniemi, R. J. (1997). Signal-space projection method for separating MEG or EEG into components. *Medical & Biological Engineering & Computing*, *35*, 135–140. https://doi.org/10.1007/BF02534144, PubMed: 9136207
Watt, R. J. (1987). Scanning from coarse to fine spatial scales in the human visual system after the onset of a stimulus. *Journal of the Optical Society of America A*, *4*, 2006–2021. https://doi.org/10.1364/JOSAA.4.002006, PubMed: 3430211
Witzel, C. (2019). Misconceptions about colour categories. *Review of Philosophy and Psychology*, *10*, 499–540. https://doi.org/10.1007/s13164-018-0404-5
Wu, Y., Zhang, Y., Mao, Y., Feng, K., Wei, D., & Song, L. (2022). Reconstructing sources location of visual color cortex by the task-irrelevant visual stimuli through machine learning decoding. *Heliyon*, *8*, e12287. https://doi.org/10.1016/j.heliyon.2022.e12287, PubMed: 36582686
Zeki, S., & Bartels, A. (1999). The clinical and functional measurement of cortical (in)activity in the visual brain, with special reference to the two subdivisions (V4 and V4 alpha) of the human colour centre. *Philosophical Transactions of the Royal Society of London, Series B: Biological Sciences*, *354*, 1371–1382. PubMed: 10466157